ARTICLE

https://doi.org/10.1038/s41586-018-0645-6

De novo NAD$^+$ synthesis enhances mitochondrial function and improves health

Elena Katsyuba[1], Adrienne Mottis[1], Marika Zietak[2,3], Francesca De Franco[4], Vera van der Velpen[5], Karim Gariani[1,11], Dongryeol Ryu[1,12], Lucia Cialabrini[6], Olli Matilainen[1,13], Paride Liscio[4], Nicola Giacchè[4], Nadine Stokar-Regenscheit[7,14], David Legouis[8,9], Sophie de Seigneux[9,10], Julijana Ivanisevic[5], Nadia Raffaelli[6], Kristina Schoonjans[2], Roberto Pellicciari[4]* & Johan Auwerx[1]*

Nicotinamide adenine dinucleotide (NAD$^+$) is a co-substrate for several enzymes, including the sirtuin family of NAD$^+$-dependent protein deacylases. Beneficial effects of increased NAD$^+$ levels and sirtuin activation on mitochondrial homeostasis, organismal metabolism and lifespan have been established across species. Here we show that α-amino-β-carboxymuconate-ε-semialdehyde decarboxylase (ACMSD), the enzyme that limits spontaneous cyclization of α-amino-β-carboxymuconate-ε-semialdehyde in the de novo NAD$^+$ synthesis pathway, controls cellular NAD$^+$ levels via an evolutionarily conserved mechanism in *Caenorhabditis elegans* and mouse. Genetic and pharmacological inhibition of ACMSD boosts de novo NAD$^+$ synthesis and sirtuin 1 activity, ultimately enhancing mitochondrial function. We also characterize two potent and selective inhibitors of ACMSD. Because expression of ACMSD is largely restricted to kidney and liver, these inhibitors may have therapeutic potential for protection of these tissues from injury. In summary, we identify ACMSD as a key modulator of cellular NAD$^+$ levels, sirtuin activity and mitochondrial homeostasis in kidney and liver.

Increasing NAD$^+$ levels activate the sirtuins and have a positive effecct on metabolism in different model organisms[1–4]. Given the beneficial effects of replenished NAD$^+$ pools, there is an intense search for strategies to increase intracellular NAD$^+$ by limiting NAD$^+$ consumption or increasing NAD$^+$ production[5]. NAD$^+$ can be produced via salvage pathways or by de novo synthesis. De novo NAD$^+$ synthesis starts from the amino acid tryptophan[6]. The formation of unstable α-amino-β-carboxymuconate-ε-semialdehyde (ACMS) constitutes a branching point of this pathway (Extended Data Fig. 1a). ACMS undergoes either cyclization, forming the NAD$^+$ precursor quinolinic acid, or total oxidation to CO_2 and H_2O. Whereas the cyclization of ACMS occurs spontaneously, the transformation of ACMS to α-amino-β-muconate-ε-semialdehyde (AMS) is catalysed by ACMSD, which determines the proportion of ACMS able to undergo cyclization and produce NAD$^+$. ACMSD is conserved across species, with mouse, rat and *C. elegans* (ACSD-1, Y71D11A.3) orthologues showing 85, 85 and 48% similarity, respectively, to the human protein[7]. On the basis of this sequence conservation, we initially characterized the function of ACSD-1 in *C. elegans*.

acsd-1 controls NAD$^+$ levels in *C. elegans*

The newly generated *C. elegans acsd-1*::GFP reporter strain showed expression of *acsd-1* in the majority of tissues throughout development and adulthood (Extended Data Fig. 1b, c). *acsd-1* RNA-mediated interference (RNAi)—by feeding worms with HT115 *Escherichia coli* that expresses *acsd-1* RNA—decreased *acsd-1* transcript levels by 46% in wild-type (N2) worms, and by 78% in *rrf-3(pk1426)* mutant worms, which are hypersensitive to RNAi (Extended Data Fig. 1d). *acsd-1* RNAi resulted in complete loss of function (LOF) of ACSD-1 enzymatic activity in *rrf-3* mutants and 70% loss of ACSD-1 activity in N2 worms (Extended Data Fig. 1e).

It has long been postulated[8,9], on the basis that they do not possess a quinolinate phosphoribosyltransferase (QPRT) orthologue with obvious sequence similarities (Extended Data Fig. 1a), that *C. elegans* cannot synthesize NAD$^+$ de novo and therefore rely on pre-formed pyridine rings to produce NAD$^+$. This was recently disproved, as uridine monophosphate synthetase replaces this function of QPRT in the nematode[10]. We detected QPRT-like enzymatic activity in both N2 and *rrf-3* worms (Extended Data Fig. 1f), and showed that tryptophan dose-dependently increased NAD$^+$ levels (Fig. 1a). Finally, *acsd-1* RNAi increased NAD$^+$ content 1.2-fold (Fig. 1b).

Increases in NAD$^+$ are known to extend lifespan of worms[11,12]. *acsd-1* RNAi did not affect N2 lifespan in basal conditions (Extended Data Fig. 1g), but survival of *rrf-3* mutants was significantly increased (Extended Data Fig. 1h). The lifespan-enhancing effect therefore seems to depend on the extent of *acsd-1* downregulation. Consistent with

[1]Laboratory of Integrative and Systems Physiology, Interfaculty Institute of Bioengineering, École Polytechnique Fédérale de Lausanne, Lausanne, Switzerland. [2]Laboratory of Metabolic Signaling, Interfaculty Institute of Bioengineering, École Polytechnique Fédérale de Lausanne, Lausanne, Switzerland. [3]Institute of Animal Reproduction and Food Research, Polish Academy of Sciences, Olsztyn, Poland. [4]TES Pharma, Loc. Taverne, Corciano, Italy. [5]Metabolomics Platform, Faculty of Biology and Medicine, University of Lausanne, Lausanne, Switzerland. [6]Department of Agricultural, Food and Environmental Sciences, Polytechnic University of Marche, Ancona, Italy. [7]Histology Core Facility, École Polytechnique Fédérale de Lausanne, Lausanne, Switzerland. [8]Intensive Care Unit, Department of Anaesthesiology, Pharmacology and Intensive Care, University Hospital of Geneva, Geneva, Switzerland. [9]Laboratory of Nephrology, Department of Internal Medicine Specialties and Department of Cell Physiology and Metabolism, University of Geneva, Geneva, Switzerland. [10]Service of Nephrology, Department of Internal Medicine Specialties, University Hospital of Geneva, Geneva, Switzerland. [11]Present address: Service of Endocrinology, Diabetes, Hypertension and Nutrition, Geneva University Hospitals, Geneva, Switzerland. [12]Present address: Molecular and Integrative Biology Lab, Healthy Aging-Korean Medical Research Center, Department of Korean Medical Science, School of Korean Medicine, Pusan National University, Yangsan, South Korea. [13]Present address: Institute of Biotechnology, University of Helsinki, Helsinki, Finland. [14]Present address: Roche Pharma Research and Early Development, Pharmaceutical Sciences, Roche Innovation Center Basel, F. Hoffmann-La Roche, Basel, Switzerland. *e-mail: rpellicciari@tespharma.com; admin.auwerx@epfl.ch

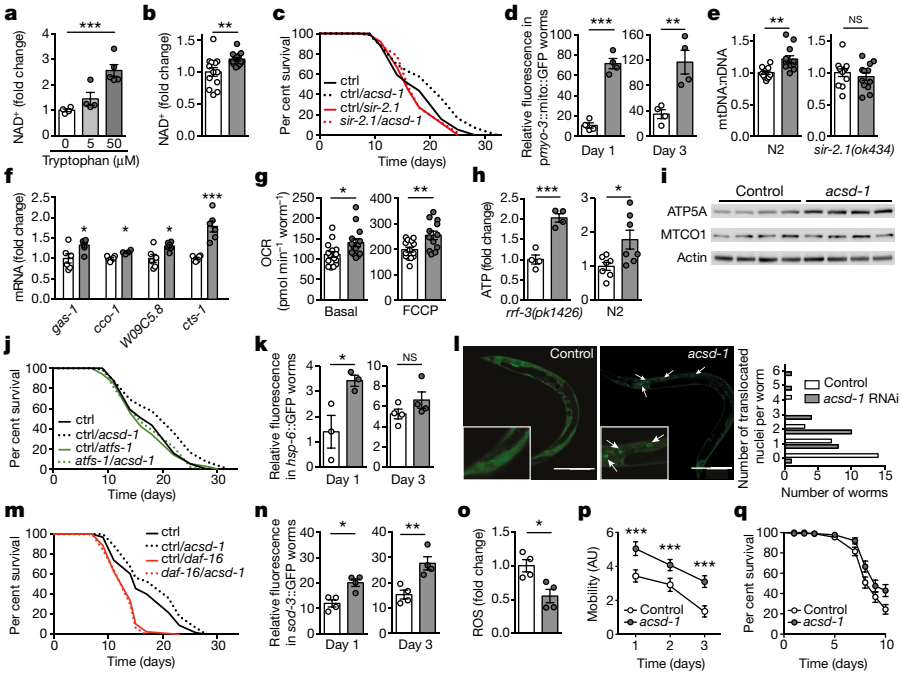

Fig. 1 | *acsd-1* LOF increases NAD^+ levels, improves mitochondrial function and increases lifespan through de novo synthesis in *C. elegans*. **a**, **b**, Increase in NAD^+ levels in worms with tryptophan supplementation (**a**; $n = 4$ (0 and 5 μM), $n = 5$ (50 μM)) and feeding with control (empty vector) or *acsd-1* RNAi (**b**; $n = 14$). Each n represents a pool of ~1,000 worms. **c**, Epistasis of *acsd-1* with *sir-2.1* RNAi. Control versus ctrl + *acsd-1* RNAi, $P < 0.0001$; ctrl + *sir-2.1* RNAi versus *sir-2.1* RNAi + *acsd-1* RNAi, not significant. **d**, GFP signal in the reporter strain, expressing a mitochondria-targeted GFP in muscle at day 1 and 3 of adulthood ($n = 4$ pools of 20 worms). **e**, mtDNA:nDNA ratio in wild-type (N2) and *sir-2.1(ok434)* mutant worms ($n = 12$ worms) with control or *acsd-1* RNAi. **f**, **g**, Changes in expression of mRNA encoding mitochondrial proteins (**f**; $n = 6$ pools of ~600 worms) and oxygen consumption rate (OCR) in basal and uncoupled conditions (**g**; $n = 14$ pools of 10 worms) in worms fed with control or *acsd-1* RNAi. **h**, ATP content in *rrf-3(pk1426)* and N2 worms fed with control (empty vector) or *acsd-1* RNAi ($n = 4$ or 7 pools of ~100 worms, respectively). **i**, Expression of OXPHOS subunits encoded by nDNA (ATP5A) and mtDNA (MTCO1) with control or *acsd-1* RNAi. Each lane represents a pool of ~600 worms. **j**, Epistasis of *acsd-1* with the UPR^{mt} regulator *atfs-1* RNAi. Control RNAi versus ctrl + *acsd-1* RNAi, $P < 0.001$; ctrl + *atfs-1* RNAi versus *atfs-1* + *acsd-1* RNAi, not significant. **k**, GFP signal in *hsp-6*::GFP reporter strain fed with control or *acsd-1* RNAi at day 1 and 3 of adulthood (day 1, $n = 3$; day 3, $n = 4$; each n represents a pool of 20 worms). **l**, Nuclear translocation of DAF-16. Arrowheads indicate DAF-16 accumulation within nuclei. The graph represents the distribution of worms treated with control or *acsd-1* RNAi in which DAF-16 has translocated to the nuclei ($n = 25$ worms). Scale bar, 100 μm. **m**, Epistasis of *acsd-1* with *daf-16* RNAi. Control RNAi versus ctrl + *acsd-1* RNAi, $P < 0.001$; ctrl + *daf-16* RNAi versus *daf-16* + *acsd-1* RNAi, not significant. **n**, GFP signal in *sod-3*::GFP reporter worms at day 1 and 3 of adulthood treated with control and *acsd-1* RNAi ($n = 4$ pools of 20 worms). **o**, ROS in worms exposed to control or *acsd-1* RNAi ($n = 4$ pools of 20 worms). **p**, **q**, Mobility (**p**) and survival (**q**; $P = 0.003$) in N2 worms exposed to 4 mM paraquat starting from L4 stage, treated with control or *acsd-1* RNAi throughout their life ($n = 100$ worms). All worm assays were performed at 20 °C and repeated at least once. Data are mean ± s.e.m. $*P \leq 0.05$, $**P \leq 0.01$, $***P \leq 0.001$; NS, not significant. P values calculated using one-way ANOVA (**a**), two-tailed t-test (**b**, **d**–**h**, **k**, **n**–**p**) or log-rank test (**c**, **j**, **m**, **q**). For gel source images, see Supplementary Fig. 1. For individual P values, see Source Data. For lifespan values, see Extended Data Table 1. AU, arbitrary units.

reported data[13], and with the effects of tryptophan supplementation on NAD^+ concentration, tryptophan also extended worm lifespan, and *acsd-1* RNAi did not result in a significant further extension beyond the effects of tryptophan alone (Extended Data Fig. 1i). Although the effects of *sir-2.1* overexpression on lifespan are disputed[14,15], *sir-2.1* has been shown to have a role in NAD^+-mediated lifespan extension[11,12]. Accordingly, we found that *sir-2.1* was required for the longevity effect of *acsd-1* RNAi (Fig. 1c), supporting the role of *sir-2.1* in NAD^+-dependent lifespan regulation. As ACSD-1 is involved in several molecular pathways, the effects upon loss of its function may not be mediated exclusively by changes in NAD^+ levels, but could also arise partly from changes in the levels of products of ACSD-1 enzymatic activity, such as AMS or picolinic acid. The contribution of these downstream factors remains to be determined.

Sirtuin activation is associated with enhanced mitochondrial function[1,2]. *acsd-1* RNAi in the *myo-3*::GFP(mit) and *ges-1*::GFP(mit) reporter strains—which express mitochondria-targeted GFP in muscle and intestinal cells, respectively—robustly increased mitochondrial content in both tissues (Fig. 1d, Extended Data Fig. 1j). Measurement of the ratio of mitochondrial DNA (mtDNA) to nuclear DNA (nDNA) confirmed the increase in mitochondria upon *acsd-1* RNAi in wild-type worms, but not in *sir-2.1(ok434)* mutants (Fig. 1e). Furthermore, *acsd-1* LOF increased transcript levels of many mitochondrial genes, basal and maximal respiration, mitochondrial complex II levels and ATP content (Fig. 1f–h, Extended Data Fig. 1k). The mitochondrial network was also more extensive and interconnected in worms treated with *acsd-1* RNAi (Extended Data Fig. 1l).

acsd-1 LOF activates mitochondrial stress defence

Notably, *acsd-1* RNAi induced expression of proteins associated with oxidative phosphorylation (OPXPHOS) and proteins encoded by nDNA, such as H28O16.1 (an orthologue of mammalian ATP5A), whereas expression of OXPHOS components encoded by mtDNA—such as MTCE.26 (an orthologue of mammalian MTCO1)—was unchanged (Fig. 1i). Changes in the ratio of proteins encoded by mtDNA versus nDNA are a hallmark of mitonuclear protein imbalance, which can be induced by increasing NAD^+ concentrations[11] and which is associated with the activation of the mitochondrial unfolded protein response (UPR^{mt})[16]. LOF of either *atfs-1* or *ubl-5*—which are essential UPR^{mt} genes[17,18]—attenuated the increased longevity resulting from *acsd-1* RNAi alone (Fig. 1j, Extended Data Fig. 1m), indicating that the UPR^{mt} is required for the lifespan extension effect. By using *hsp-6*::GFP, a reporter for a mitochondrial chaperone orthologous to mammalian mtHsp70, we observed a robust activation of the UPR^{mt}

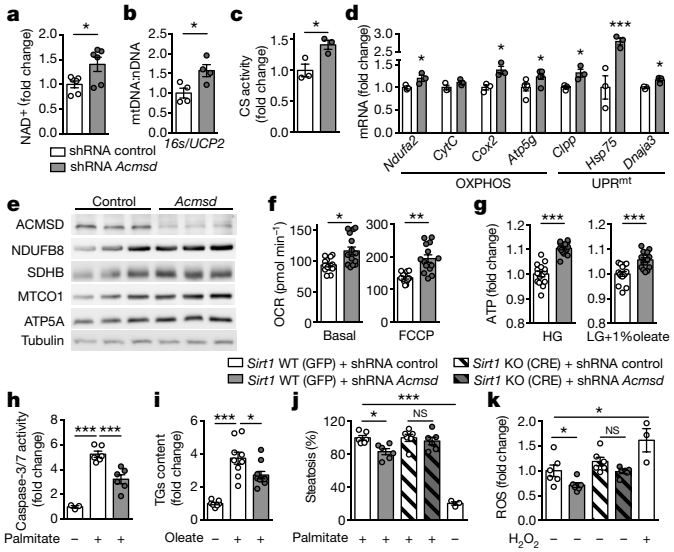

Fig. 2 | Pathways activated by *Acmsd* knockdown in worms are conserved in mammalian cells. a–f, Mouse primary hepatocytes obtained from C57BL/6J mice were transduced with an adenovirus encoding either control shRNA or shRNA directed against *Acmsd* for 48 h. Change in NAD^+ levels ($n = 6$) (**a**), mtDNA:nDNA ratio ($n = 4$) (**b**), citrate synthase (CS) activity ($n = 3$) (**c**), expression of OXPHOS and UPR^{mt} genes ($n = 3$) (**d**), protein expression of respiratory complex subunits (**e**) and oxygen consumption in basal and uncoupled (2 μM *p*-trifluoromethoxy carbonyl cyanide phenyl hydrazone (FCCP)) conditions ($n = 15$) (**f**). **g**, Change in ATP levels in mouse primary hepatocytes grown in both medium with high glucose (HG) or low glucose (LG) supplemented with 1% oleate treated with control shRNA versus *Acmsd* shRNA ($n = 15$). **h**, Apoptosis evaluated by caspase-3/7 activity after 24-h exposure of mouse primary hepatocytes to 0.75 mM palmitate (no palmitate, $n = 3$; palmitate, $n = 6$). **i**, Triglyceride (TGs) content after 24-h exposure to 0.5 mM oleate in AML12 cells transduced with an adenovirus encoding either control or *Acmsd* shRNA ($n = 9$). **j**, **k**, Primary hepatocytes extracted from a $Sirt1^{L2/L2}$ mouse transduced with an adenovirus encoding either GFP (wild-type) or Cre recombinase (to generate *Sirt1* knockout (KO) primary hepatocytes). **j**, Steatosis in hepatocytes treated with control or *Acmsd* shRNA after 24-h exposure to 0.75 mM palmitate (no palmitate, $n = 3$; palmitate, $n = 6$). **k**, ROS content in hepatocytes exposed to control shRNA versus *Acmsd* shRNA. The positive control is treated with 550 μM H_2O_2 (no H_2O_2, $n = 3$; H_2O_2, $n = 6$). Data are mean ± s.e.m.; *n* represents number of biologically independent samples. All experiments performed independently at least twice. $*P \leq 0.05$, $**P \leq 0.01$, $***P \leq 0.001$. *P* values calculated using two-tailed *t*-test (**a**–**d**, **f**–**i**) or two-way ANOVA (**j**–**k**). For gel source images, see Supplementary Fig. 1. For individual *P* values, see Source Data.

upon *acsd-1* RNAi (Fig. 1k). This stress response was specific, as there was no activation of the unfolded protein response in the endoplasmic reticulum or of the cytosolic heat shock response in *hsp-4*::GFP and *hsp-16.2*::GFP reporter strains, respectively, after *acsd-1* LOF (Extended Data Fig. 1n–o). Several UPR^{mt}-related transcripts were induced upon *acsd-1* RNAi (Extended Data Fig. 1p).

In *C. elegans*, oxidative stress defence is launched when DAF-16—an orthologue of forkhead box O transcription factor (FOXO)—is translocated into the nucleus[19], where it induces the mitochondrial superoxide dismutase[20] *sod-3*. Supplementing *C. elegans* with NAD^+ was reported to activate oxidative stress defence and to improve resistance to reactive oxygen species (ROS) in a *sir-2.1*- and *daf-16*-dependent fashion[12]. Consistent with this mechanism, DAF-16 translocated into nuclei upon *acsd-1* LOF (Fig. 1l). The increased lifespan as a result of *acsd-1* RNAi was lost upon *daf-16* LOF (Fig. 1m). Consistent with increased nuclear localization of DAF-16, *acsd-1* LOF increased the GFP signal in *sod-3*::GFP reporter worms as well as *sod-3* expression (Fig. 1n, Extended Data Fig. 1q). As a consequence, worms with *acsd-1* knockdown had reduced levels of ROS, were more active and lived longer when exposed to paraquat, a known ROS inducer (Fig. 1o–q). The increased survival under paraquat was independent of the developmental stage at which worms were exposed to *acsd-1* RNAi, but required *daf-16* (Extended Data Fig. 1r, s).

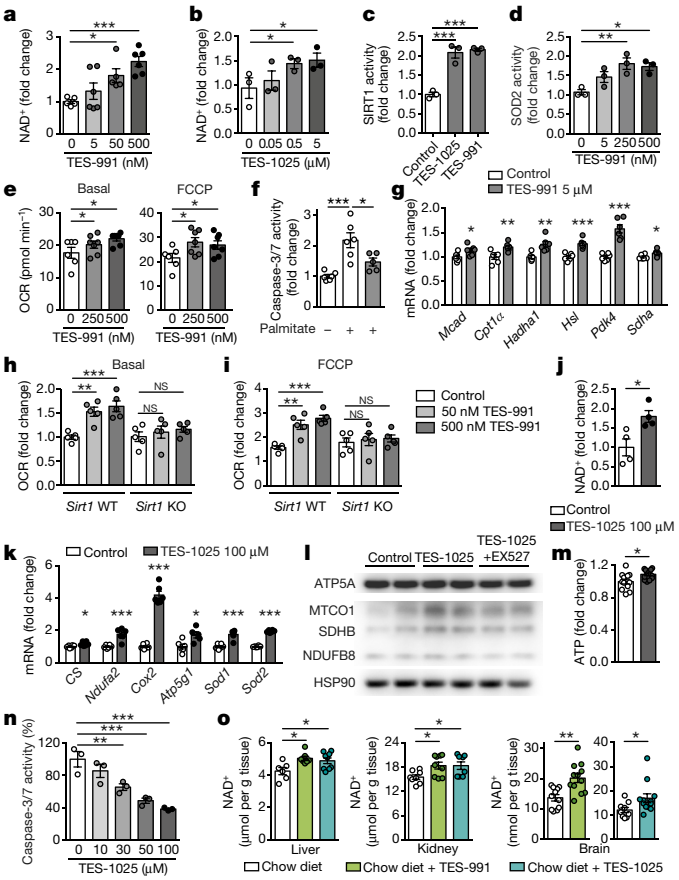

Fig. 3 | Pharmacological inhibition of ACMSD has similar effects to genetic downregulation. a, **b**, NAD^+ levels in mouse primary hepatocytes treated for 24 h with vehicle (dimethyl sulfoxide, DMSO), TES-991 ($n = 6$) (**a**) or TES-1025 ($n = 3$) (**b**). **c**, SIRT1 activity in primary hepatocytes treated for 24 h with vehicle or 500 nM TES-1025 or TES-991 ($n = 3$). **d**–**f**, SOD2 activity ($n = 3$) (**d**), oxygen consumption in basal and uncoupled conditions (ctrl, $n = 6$; TES-991, $n = 7$) (**e**) and apoptosis rate after 36 h exposure to 0.75 mM palmitate (ctrl, $n = 6$; TES-991, $n = 5$) (**f**) in primary hepatocytes treated for 24 h with vehicle or TES-991. **g**, mRNA levels of fatty acid oxidation (FAO) genes in primary hepatocytes treated with vehicle or 500 nm TES-991 after 6 h exposure to 0.33 mM palmitate and 0.66 mM oleate ($n = 6$). **h**, **i**, Primary hepatocytes from a $Sirt1^{L2/L2}$ mouse transduced with an adenovirus encoding GFP (*Sirt1* WT) or Cre recombinase (*Sirt1* KO). FAO after 24-h treatment with vehicle or TES-991 under basal (**h**) or uncoupled (**i**) conditions ($n = 5$). **j**–**m**, Changes in NAD^+ ($n = 4$) (**j**), mRNA levels of mitochondrial and oxidative stress defence genes ($n = 6$) (**k**), protein levels of OXPHOS subunits (**l**) and ATP content (ctrl, $n = 12$; TES-1025, $n = 13$) (**m**) in HK-2 cells upon treatment with 100 μM TES-1025, or TES-1025 in combination with 10 μM SIRT1 inhibitor EX527, for 24 h. **n**, Apoptosis in HK-2 cells 16 h after addition of 50 μM cisplatin. TES-1025 was added 1 h before cisplatin ($n = 3$). **o**, NAD^+ in livers (ctrl, $n = 6$; TES-991, $n = 7$; TES-1025, $n = 9$ mice), kidneys (ctrl, TES-1025, $n = 8$; TES-991, $n = 9$ mice) and brains (ctrl, $n = 11$; TES-991, TES-1025, $n = 12$ mice) of mice fed with normal chow diet or supplemented with ACMSD inhibitors (15 mg kg^{-1} body weight day^{-1}). Data are mean ± s.e.m.; each *n* represents a biologically independent sample. Experiments in **a**–**n** performed independently at least twice. $*P \leq 0.05$, $**P \leq 0.01$, $***P \leq 0.001$. *P* values calculated using two-tailed *t*-test (**a**–**c**, **f**, **g**, **j**, **k**, **m**–**o**), or one-way (**d**, **e**) or two-way ANOVA (**h**, **i**). For gel source images, see Supplementary Fig. 1. For individual *P* values, see Source Data.

ACMSD function is conserved in mammals

We next investigated whether the molecular mechanisms observed in *C. elegans* upon *acsd-1* LOF are evolutionarily conserved. In humans,

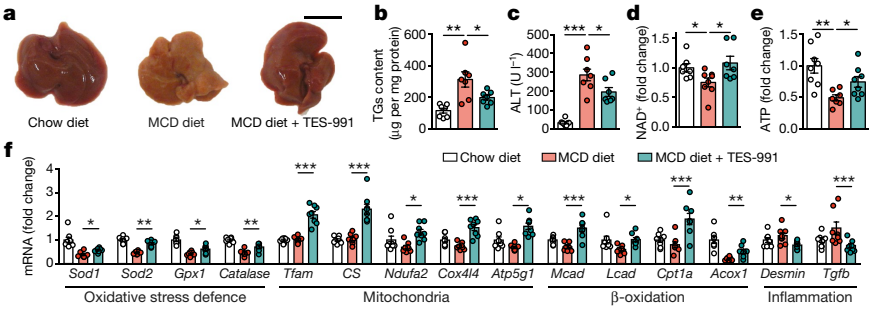

Fig. 4 | ACMSD inhibitors protect hepatic function from MCD diet-induced NAFLD. a, Comparison of gross liver morphology in representative 16-week-old C57BL/6J male mice fed for 2.5 weeks with control diet, MCD diet or MCD diet supplemented with 15 mg kg^{-1} day^{-1} of TES-991. The in vivo MCD diet study was performed once. Scale bar, 1 cm. **b**–**e**, Liver triglycerides (**b**), plasma ALT (**c**), liver NAD^+ (**d**) and ATP (**e**) levels in the mouse cohorts described in **a** (control diet, MCD, $n = 8$; MCD + TES-991, $n = 7$ mice). **f**, mRNA levels of oxidative stress defence, mitochondrial, β-oxidation, inflammatory and fibrosis genes in livers of the mice described in **a** ($n = 8$ mice). *Lcad* is also known as *Acadl*, *Tgfb* is also known as *Tgfb1* and *Mcad* is also known as *Acadm*. Data are mean ± s.e.m. $*P \leq 0.05$, $**P \leq 0.01$, $***P \leq 0.001$. *P* values calculated using two-tailed *t*-test. For individual *P* values, see Source Data.

ACMSD was mainly detected in liver and kidney. Some *Acmsd* transcripts were present in brain, 1300- and 30-fold lower than in kidney and liver, respectively[21]; this is in line with data in the Human Protein Atlas[22] (http://www.proteinatlas.org/ENSG00000153086-ACMSD/tissue). Mouse primary hepatocytes exhibited higher levels of *Acmsd* expression than the tested mouse (AML-12, Hepa 1-6) and human (HepG2, HuH-7, HEK 293, HK-2) hepatic and renal cell lines (Extended Data Fig. 2a), and were therefore selected for further study.

Acmsd expression was reduced by more than 98% in mouse primary hepatocytes transduced with an adenovirus encoding a short hairpin RNA (shRNA) targeting *Acmsd* (Extended Data Fig. 2b). Consistent with our *C. elegans* data, total cellular NAD^+ was 1.4-fold higher in hepatocytes treated with *Acmsd* shRNA compared to hepatocytes transduced with scrambled control shRNA (Fig. 2a), whereas there was no detectable effect on mitochondrial NAD^+ (Extended Data Fig. 2c). *Acmsd* downregulation also enhanced mitochondrial function in hepatocytes, as indicated by increased mtDNA:nDNA ratio, citrate synthase activity and expression of OXPHOS genes both at the transcript and protein levels (Fig. 2b–e). In-gel activity assays for complex I and complex IV showed overall increased activity in cells treated with *Acmsd* shRNA, including in high molecular mass supercomplexes (Extended Data Fig. 2d, e). *Acmsd* shRNA also increased levels of UPR^{mt} transcripts (Fig. 2d) and basal and maximal oxygen consumption rate and ATP concentration in mouse primary hepatocytes grown in high or low glucose (Fig. 2f, g).

In sum, these changes indicate that hepatocyte mitochondrial function was improved by *Acmsd* LOF; we therefore tested whether knocking down *Acmsd* could render hepatocytes more resilient to steatosis and apoptosis caused by high fatty acid concentration. LOF of *Acmsd* protected primary mouse hepatocytes from fatty acid-induced apoptosis (Fig. 2h) and attenuated triglyceride accumulation (Fig. 2i); this effect was dependent on sirtuin 1 (SIRT1) (Fig. 2j, Extended Data Fig. 2f). *Acmsd* shRNA also reduced levels of ROS in primary hepatocytes in a SIRT1-dependent manner (Fig. 2k) and lowered acetylation levels of FOXO1, a deacetylation target of SIRT1 (Extended Data Fig. 2g).

Characterization of ACMSD inhibitors

The first indications that inhibiting ACMSD activity could enhance de novo NAD^+ synthesis came from studies on phthalate esters and pyrazinamide; however, these compounds have pleiotropic effects[23,24]. We therefore developed selective and potent ACMSD inhibitors, TES-991 and TES-1025[25], and investigated their therapeutic potential. Similar to genetic *Acmsd* LOF, pharmacological inhibition of ACMSD with either compound dose-dependently increased NAD^+ levels and resulted in SIRT1 activation in primary hepatocytes (Fig. 3a–c). Both ACMSD inhibitors induced mitochondrial transcripts and enhanced both basal and maximal oxygen consumption rate and mitochondrial SOD2 activity in primary mouse hepatocytes (Fig. 3d, e, Extended Data Fig. 3a–c). Similar to genetic *Acmsd* LOF, ACMSD inhibition protected primary hepatocytes from apoptosis induced by high doses of fatty acids (Fig. 3f) and promoted fatty acid oxidation in a SIRT1-dependent manner; this was confirmed by both induction of β-oxidation genes and functional assays (Fig. 3g–i, Extended Data Fig. 3d).

TES-1025, the inhibitor with the best exposure profile for the kidney[25], also increased NAD^+ content in human HK-2 kidney cells (Fig. 3j). TES-1025 induced transcription of mitochondrial and ROS defence genes, as well as protein levels of the OXPHOS subunits in a SIRT1-dependent manner (Fig. 3k, l, Extended Data Fig. 3e). Treatment of HK-2 cells with TES-1025 also increased their ATP content (Fig. 3m). Cisplatin-induced apoptosis was attenuated when HK-2 cells were either pre-treated with (Fig. 3n) or exposed to TES-1025 simultaneously with cisplatin (Extended Data Fig. 3f).

We next characterized the effect of both compounds in the mouse. Feeding 9-week-old male C57BL/6J mice for 10 days with chow diet supplemented with TES-991 or TES-1025 (15 mg kg^{-1} body weight day^{-1}) did not result in any pronounced effects on metabolic homeostasis and did not otherwise affect liver or kidney function (Extended Data Fig. 3g). Both TES-991 and TES-1025 increased NAD^+ content in liver, kidneys and brain (Fig. 3o), whereas NAD^+ levels in heart and skeletal muscle seemed unaffected (not shown). Changes in quinolinic acid did not show a consistent pattern after pharmacological inhibition of ACMSD. Whereas in brain, quinolinic acid concentration tended to increase (statistically significant for TES-1025, but to concentrations too low to provoke neurotoxicity[26]), levels were reduced in kidney and unchanged in liver (Extended Data Fig. 3h). Both ACMSD inhibitors caused depletion of nicotinic acid in liver, kidney and brain, which could serve as another readout for ACMSD inhibition (Extended Data Fig. 3i). Besides this, administration of ACMSD inhibitors induced transcription of mitochondrial genes in the liver, whereas the expression of the same genes in the kidneys was unaffected (Extended Data Fig. 3j, k).

Efficacy of ACMSD inhibitors in disease models

On the basis of the observed differences in exposure profiles of the two ACMSD inhibitors, with TES-991 being enriched in liver and TES-1025 in the kidney[25], we assessed the translational potential of TES-991 in the setting of liver disease and oriented in vivo studies with TES-1025 to the kidney. Non-alcoholic fatty liver disease (NAFLD) is the most common liver disease worldwide, often leading to progressive liver damage, termed non-alcoholic steatohepatitis[27]. Given the efficacy of boosting NAD^+ to attenuate NAFLD in mouse models[28,29], we tested the efficacy of ACMSD inhibition in a mouse model of NAFLD, induced by feeding 13-week-old C57BL/6J mice with a methionine-choline-deficient (MCD) diet for 2.5 weeks[29]. Supplementing the MCD diet with TES-991 (15 mg kg^{-1} day^{-1} prophylactically) attenuated hepatic

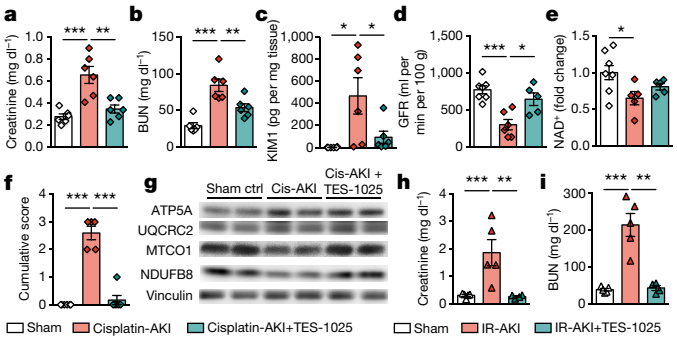

Fig. 5 | ACMSD inhibitors protect renal function in two different models of AKI. a–**c**, Plasma creatinine (**a**), BUN (**b**) and renal KIM1 protein levels (**c**) in 12-week-old C57BL/6J male mice 72 h after cisplatin administration. AKI was induced at day 10 after the beginning of the study by a single intraperitoneal injection of cisplatin (20 mg kg^{-1} body weight). Sham controls were injected with saline solution; TES-1025 was administered at 15 mg kg^{-1} body weight day^{-1} ($n = 6$ mice). **d**, Glomerular filtration rate (GFR) in mice 52 h after cisplatin or saline administration (sham, $n = 7$; cisplatin, $n = 6$; cisplatin + TES-1025, $n = 5$ mice). **e**, NAD^+ levels in kidneys of the cisplatin-AKI mice (sham, $n = 7$; cisplatin, cisplatin + TES-1025, $n = 5$ mice). **f**, Histopathological scoring of haematoxylin and eosin (H&E)-stained kidney sections from mice described in **a**, showing tubular necrosis, tubular dilation, inflammation, oedema and cast (sham, cisplatin + TES-1025, $n = 6$; cisplatin, $n = 5$ mice). Scoring was performed by two pathologists in a blinded and independent way. **g**, Protein expression of respiratory complex subunits in kidneys from mouse cohorts described in **a**. The experiment was performed twice. Cis, cisplatin. **h**, **i**, AKI was induced in 12-week-old C57BL/6J male mice by a dorsal surgical incision and bilateral occlusion of the renal pedicles for 25 min; a simple dorsal incision was performed for the sham controls. TES-1025 was administered at 15 mg kg^{-1} day^{-1}. Plasma creatinine (**h**) and BUN (**i**) in mice 48 h after surgery ($n = 5$ mice). Data are mean ± s.e.m. $^*P \leq 0.05$, $^{**}P \leq 0.01$, $^{***}P \leq 0.001$. *P* values calculated using two-tailed *t*-test. For gel source images, see Supplementary Fig. 1. For individual *P* values, see Source Data.

steatosis (Fig. 4a, b) and plasma alanine transaminase (ALT) and aspartate transaminase levels (Fig. 4c, Extended Data Fig. 4a). As expected, the MCD diet depleted the hepatic NAD^+ pool; this effect was reversed by TES-991 (Fig. 4d). TES-991 also protected against hepatic lipid accumulation and attenuated inflammation (Extended Data Fig. 4b, c). Hepatic SOD2 activity and ATP content, which were reduced with the MCD diet, also partially recovered with TES-991 (Fig. 4e, Extended Data Fig. 4d). Furthermore, inhibition of ACMSD reversed changes in transcription of genes involved in ROS defence, β-oxidation, inflammation and mitochondrial function, which are known to be modulated in NAFLD (Fig. 4f). Whereas supplementation of the MCD diet with TES-991 was still able to increase hepatic NAD^+ in *Sirt1* knockout (*Sirt1*$^{hep-/-}$) mice (Extended Data Fig. 4e), TES-991 no longer protected the *Sirt1*$^{hep-/-}$ livers from NAFLD induced by MCD diet, as reflected in the hepatic lipid content, plasma markers of liver damage, SOD2 activity and changes in liver transcript levels (Extended Data Fig. 4f–k).

Acute kidney injury (AKI) affects 3–7% of all hospitalized patients and has a high mortality rate, especially when it occurs in the setting of intensive care[30]. A recent study found that increased NAD^+ levels can provide protection against AKI[31]. Following our observation of a protective effect of ACMSD inhibitors in cisplatin-challenged HK-2 cells, we investigated the effect of ACMSD inhibition in a mouse model of AKI, induced by application of single intraperitoneal dose of cisplatin to 12-week-old male C57BL/6J mice (Extended Data Fig. 5a). Supplementation of chow diet with TES-1025 (15 mg kg^{-1} day^{-1} given prophylactically), protected against AKI, as indicated by the normalization of blood creatinine, blood urea nitrogen (BUN) and KIM1 levels (Fig. 5a–c). Glomerular filtration rate was severely compromised after cisplatin challenge in vehicle-treated animals, but was preserved in mice receiving TES-1025 (Fig. 5d). Whereas the administration of cisplatin depleted renal NAD^+ levels, this drop in NAD^+ was less pronounced in mice treated with TES-1025 (Fig. 5e). Consistent with these biochemical indications of improved function, the increase in cumulative histopathological score—which evaluates tubular necrosis, tubular dilation, inflammation, oedema and cast formation—was also reduced by ACMSD inhibition (Fig. 5f, Extended Data Fig. 5b–d). TES-1025 also restored the cisplatin-induced changes in expression of OXPHOS complexes in the kidney (Fig. 5g).

We further confirmed the protective effects of TES-1025 (15 mg kg^{-1} body weight day^{-1}) in a distinct AKI model; ischaemia-reperfusion AKI (IR-AKI). Renal pedicles of 12-week-old male C57BL/6J mice were clamped for 25 min to induce mild-to-moderate AKI (Extended Data Fig. 5e). Similar to the cisplatin-induced AKI model, administration of TES-1025 protected from structural and functional renal damage inflicted by IR-AKI (Fig. 5h, i, Extended Data Fig. 5f–j). Glutathione depletion—caused by IR-AKI—was rescued and myeloperoxidase activity, reflecting neutrophil infiltration, was attenuated by TES-1025 (Extended Data Fig. 5k, l). Furthermore, increased NAD^+ levels were detected in kidneys of mice receiving TES-1025 (Extended Data Fig. 5m). TES-1025 also normalized the renal expression of OXPHOS complexes, which was impaired by ischaemia-reperfusion (Extended Data Fig. 5n).

Conclusions

Accumulating evidence supporting a key role of robust NAD^+ homeostasis in protection against ageing and numerous diseases stimulated an interest in approaches to maintain and/or increase tissue NAD^+ levels[5]. Whereas the translational potential of increasing NAD^+ produced from precursor molecules via salvage pathways has been extensively studied, little is known about the possibility of increasing NAD^+ via the de novo NAD^+ synthesis pathway. Recent reports emphasizing the role of de novo NAD^+ biosynthesis in maintenance of whole-body NAD^+ homeostasis have identified this pathway as a target to boost NAD^+ content[32,33].

Our data position the evolutionarily conserved enzyme ACMSD as a key regulator on the de novo NAD^+ synthesis pathway. We show that ACMSD acts as a tissue-selective modulator of cellular NAD^+ levels, sirtuin activity and mitochondrial homeostasis in *C. elegans* and mouse. The high expression levels of ACMSD in the kidney and liver in mammals suggests the therapeutic potential of ACMSD inhibition for diseases of these organs such as NAFLD, non-alcoholic steatohepatitis, AKI and chronic kidney disease, which—despite their high prevalence—represent large unmet medical needs. We demonstrate beneficial effects of two potent and selective ACMSD inhibitors in animal models of NAFLD and AKI. In vivo ACMSD inhibition is associated with increases in tissue NAD^+ levels and SIRT1 activation. The ACMSD inhibitors were well-tolerated in mice and devoid of systemic side effects such as the accumulation of the potentially neurotoxic metabolite quinolinic acid[26]. In sum, our data support further investigations into the long-term benefits of ACMSD inhibition in a broader range of disease models and potential future translation of ACMSD inhibition in a clinical setting.

Online content

Any methods, additional references, Nature Research reporting summaries, source data, statements of data availability and associated accession codes are available at https://doi.org/10.1038/s41586-018-0645-6.

Received: 18 September 2017; Accepted: 18 September 2018;
Published online 24 October 2018.

1. Houtkooper, R. H., Pirinen, E. & Auwerx, J. Sirtuins as regulators of metabolism and healthspan. *Nat. Rev. Mol. Cell Biol.* **13**, 225–238 (2012).
2. Imai, S. & Guarente, L. It takes two to tango: NAD^+ and sirtuins in aging/longevity control. *NPJ Aging Mech. Dis.* **2**, https://doi.org/10.1038/npjamd.2016.17 (2016).
3. Belenky, P., Bogan, K. L. & Brenner, C. NAD^+ metabolism in health and disease. *Trends Biochem. Sci.* **32**, 12–19 (2007).

4. Yang, Y. & Sauve, A. A. NAD^+ metabolism: bioenergetics, signaling and manipulation for therapy. *Biochim. Biophys. Acta* **1864**, 1787–1800 (2016).
5. Katsyuba, E. & Auwerx, J. Modulating NAD^+ metabolism, from bench to bedside. *EMBO J.* **36**, 2670–2683 (2017).
6. Bender, D. A. Biochemistry of tryptophan in health and disease. *Mol. Aspects Med.* **6**, 101–197 (1983).
7. Fukuoka, S. I. Identification and expression of a cDNA encoding human α-amino-β-carboxymuconate-ε-semialdehyde decarboxylase (ACMSD). A key enzyme for the tryptophan-niacine pathway and "quinolinate hypothesis". *J. Biol. Chem.* **277**, 35162–35167 (2002).
8. Vrablik, T. L., Huang, L., Lange, S. E. & Hanna-Rose, W. Nicotinamidase modulation of NAD^+ biosynthesis and nicotinamide levels separately affect reproductive development and cell survival in *C. elegans*. *Development* **136**, 3637–3646 (2009).
9. Rongvaux, A., Andris, F., Van Gool, F. & Leo, O. Reconstructing eukaryotic NAD metabolism. *BioEssays* **25**, 683–690 (2003).
10. McReynolds, M. R., Wang, W., Holleran, L. M. & Hanna-Rose, W. Uridine monophosphate synthetase enables eukaryotic de novo NAD^+ biosynthesis from quinolinic acid. *J. Biol. Chem.* (2017).
11. Mouchiroud, L. et al. The NAD^+/sirtuin pathway modulates longevity through activation of mitochondrial UPR and FOXO signaling. *Cell* **154**, 430–441 (2013).
12. Hashimoto, T., Horikawa, M., Nomura, T. & Sakamoto, K. Nicotinamide adenine dinucleotide extends the lifespan of *Caenorhabditis elegans* mediated by *sir-2.1* and *daf-16*. *Biogerontology* **11**, 31–43 (2010).
13. Gebauer, J. et al. A genome-scale database and reconstruction of *Caenorhabditis elegans* metabolism. *Cell Syst.* **2**, 312–322 (2016).
14. Burnett, C. et al. Absence of effects of Sir2 overexpression on lifespan in *C. elegans* and *Drosophila*. *Nature* **477**, 482–485 (2011).
15. Viswanathan, M. & Guarente, L. Regulation of *Caenorhabditis elegans* lifespan by *sir-2.1* transgenes. *Nature* **477**, E1–E2 (2011).
16. Houtkooper, R. H. et al. Mitonuclear protein imbalance as a conserved longevity mechanism. *Nature* **497**, 451–457 (2013).
17. Benedetti, C., Haynes, C. M., Yang, Y., Harding, H. P. & Ron, D. Ubiquitin-like protein 5 positively regulates chaperone gene expression in the mitochondrial unfolded protein response. *Genetics* **174**, 229–239 (2006).
18. Haynes, C. M., Yang, Y., Blais, S. P., Neubert, T. A. & Ron, D. The matrix peptide exporter HAF-1 signals a mitochondrial UPR by activating the transcription factor ZC376.7 in *C. elegans*. *Mol. Cell* **37**, 529–540 (2010).
19. Berdichevsky, A., Viswanathan, M., Horvitz, H. R. & Guarente, L. *C. elegans* SIR-2.1 interacts with 14-3-3 proteins to activate DAF-16 and extend life span. *Cell* **125**, 1165–1177 (2006).
20. Honda, Y. & Honda, S. The *daf-2* gene network for longevity regulates oxidative stress resistance and Mn-superoxide dismutase gene expression in *Caenorhabditis elegans*. *FASEB J.* **13**, 1385–1393 (1999).
21. Pucci, L., Perozzi, S., Cimadamore, F., Orsomando, G. & Raffaelli, N. Tissue expression and biochemical characterization of human 2-amino 3-carboxymuconate 6-semialdehyde decarboxylase, a key enzyme in tryptophan catabolism. *FEBS J.* **274**, 827–840 (2007).
22. Uhlén, M. et al. Tissue-based map of the human proteome. *Science* **347**, 1260419 (2015).
23. Fukuwatari, T. Phthalate esters enhance quinolinate production by inhibiting α-amino-β-carboxymuconate-ε-semialdehyde decarboxylase (ACMSD), a key enzyme of the tryptophan pathway. *Toxicol. Sci.* **81**, 302–308 (2004).
24. Saito, K. et al. Mechanism of increases in L-kynurenine and quinolinic acid in renal insufficiency. *Am. J. Physiol. Renal Physiol.* **279**, F565–F572 (2000).
25. Pellicciari, R. et al. α-amino-β-carboxymuconate-ε-semialdehyde decarboxylase (ACMSD) inhibitors as novel modulators of de novo nicotinamide adenine dinucleotide (NAD^+) biosynthesis. *J. Med. Chem.* **61**, 745–759 (2018).
26. Chen, Y. & Guillemin, G. J. Kynurenine pathway metabolites in humans: disease and healthy states. *Int. J. Tryptophan Res.* **2**, 1–19 (2009).
27. Michelotti, G. A., Machado, M. V. & Diehl, A. M. NAFLD, NASH and liver cancer. *Nat. Rev. Gastroenterol. Hepatol.* **10**, 656–665 (2013).
28. Gariani, K. et al. Eliciting the mitochondrial unfolded protein response by nicotinamide adenine dinucleotide repletion reverses fatty liver disease in mice. *Hepatology* **63**, 1190–1204 (2016).
29. Gariani, K. et al. Inhibiting poly-ADP ribosylation increases fatty acid oxidation and protects against fatty liver disease. *J. Hepatol.* (2016).
30. Lewington, A. J., Cerda, J. & Mehta, R. L. Raising awareness of acute kidney injury: a global perspective of a silent killer. *Kidney Int.* **84**, 457–467 (2013).
31. Tran, M. T. et al. PGC1α drives NAD biosynthesis linking oxidative metabolism to renal protection. *Nature* **531**, 528–532 (2016).
32. Liu, L. et al. Quantitative analysis of NAD synthesis-breakdown fluxes. *Cell Metab.* **27**, 1067–1080 (2018).
33. Shi, H. et al. NAD deficiency, congenital malformations, and niacin supplementation. *N. Engl. J. Med.* **377**, 544–552 (2017).

Acknowledgements We thank P. Gönczy and the *Caenorhabditis* Genetics Center for providing reagents, the Bioimaging and Optics Core Facility and the Phenotyping Unit of EPFL, N. Moullan, T. Clerc and S. Bichet for technical assistance. E.K. was supported by Fondation Romande pour la Recherche sur le Diabète. M.Z. was supported by the KNOW consortium 'Healthy Animal—Safe Food' MS&HE no. 05-1/KNOW2/2015 and the Foundation for Polish Science. This work was supported by funds from EPFL and Swiss National Science Foundation (grant 310030B_160318). J.I. acknowledges funding from the Foundation Pierre-Mercier pour la Science. We thank H. Gallant-Ayala for advice on analytical methods.

Reviewer information *Nature* thanks W. Hanna-Rose, S. Parikh, J. Tam and the other anonymous reviewer(s) for their contribution to the peer review of this work.

Author contributions E.K., J.A. and R.P. conceived and designed the project. E.K., A.M., M.Z., F.D.F., K.G., D.R. and N.G. performed experiments. P.L. synthesized ACMSD inhibitors. O.M. made the *acsd-1*::GFP *C. elegans* reporter strain. N.R. and L.C. performed activity assays for the enzymes in de novo NAD^+ biosynthesis. V.v.d.V. and J.I. performed the metabolomics and N.S.-R. carried out histopathology. S.d.S. and D.L. assisted with GFR measurements. E.K., K.S. and J.A. wrote the manuscript with the contributions from all other authors.

Competing interests J.A., R.P. and N.R. are inventors on US patent 9,708,272 (18 July, 2017), filed by TES Pharma S.r.l., Corciano, Italy. The patent covers the results obtained with the ACMSD inhibitors, TES-991 and TES-1025, described in Figs. 3–5. R.P., F.D.F., N.G. and P.L. are employed by TES Pharma.

Additional information

Extended data is available for this paper at https://doi.org/10.1038/s41586-018-0645-6.
Supplementary information is available for this paper at https://doi.org/10.1038/s41586-018-0645-6.
Reprints and permissions information is available at http://www.nature.com/reprints.
Correspondence and requests for materials should be addressed to R.P. or J.A.
Publisher's note: Springer Nature remains neutral with regard to jurisdictional claims in published maps and institutional affiliations.

METHODS

***C. elegans* experiments.** *C. elegans* strains were provided by the *Caenorhabditis* Genetics Center (University of Minnesota). Worms were maintained on nematode growth medium (NGM) agar plates seeded with *E.coli* OP50 at 20 °C, unless stated otherwise. The strains used for the experiments are the following: Bristol N2, NL2099 (*rrf-3(pk1426)II*), SJ4143 (zcIs17[*ges-1*::GFP(mit)]), SJ4103 (zcIs14[*myo-3*::GFP(mit)]), KN259 (huIs33[*sod-3*::GFP+pRF4(*rol-6(su1006)*)]), SJ4005 (zcIs4[*hsp-4*::GFP]), TJ356 (zIs356[*daf-16p*::*daf-16a*/b::GFP+*rol-6*(*su1006*)], SJ4100 (zcIs13[*hsp-6*::GFP]), VC199 (*sir-2.1(ok434)IV*). If not indicated explicitly in the text, the strain used for experiments was NL2099 (*rrf-3(pk1426)II*).

Bacterial feeding RNAi experiments were carried out as previously described[34]. Clones used were *acsd-1* (Y71D11A.3), *sir-2.1* (R11A8.4), *daf-16* (R13H8.1), *ubl-5* (F46F11.4) and *atfs-1* (ZC376.7). Clones were purchased from GeneService and their identity was confirmed by sequencing. For the double-RNAi experiments, bacterial cultures were mixed before seeding on NGM plates. The control RNAi in these experiments was diluted 50% with control empty vector RNAi bacteria.

Lifespan assays. *C. elegans* lifespan assays were carried at 20 °C as previously described[35]. One hundred worms were used per condition and scored every 2 days. Reasons for censoring were the exploded vulva phenotype or worms that crawled off the plate and were pre-established before the beginning of the experiment. Where indicated, paraquat dichloride (Sigma-Aldrich) was added on top of the agar plates to obtain the indicated final concentration. Once the paraquat solution was absorbed completely by the agar, L4 worms were transferred to these agar plates and monitored daily for 5–6 days. Tests were performed in non-blinded manner and repeated twice, unless indicated otherwise.

Mobility assessment. The movement of worms was recorded for 45 s at days 1, 3 and 5 of adulthood using a Nikon DS-L2/DS-Fi1 camera and controller setup, attached to both a computer and a standard bright-field microscope. For each condition, 5 plates of worms, with 10 worms per plate, were used. The movement of worms was calculated by taking an integral of the speed value, which was assessed by following the worm centroids with a modified version of the freely-available 'parallel worm tracker' for MATLAB[36]. The experiments were non-blinded and repeated twice.

Generation of transgenic *C. elegans* strains. *acsd-1p*::GFP expression vector was created by amplifying the 1,425-bp sequence upstream from the transcription start site of the *acsd-1* coding region by using *C. elegans* genomic DNA and 5′-gtaACATGTcagtcgacgcaaaaattgtt-3′ and 5′-gtaCCCGGGtttgattcaggaaaattataaaaatt aaatg-3′ primers. The PCR product was digested with PciI and XmaI and ligated into the PciI and AgeI-digested *pPD30.38* expression vector containing the *gfp* coding sequence cloned between inserted AgeI and NotI restriction sites. Two independent lines carrying *acsd-1p*::GFP transgene as extrachromosomal array were analysed in the study.

Imaging and image processing. Confocal images were acquired with Zeiss LSM 700 Upright confocal microscope (Carl Zeiss AG) under non-saturating exposure conditions. The worms were prepared for imaging as previously described[16]. In brief, nematodes were immobilized with 7.5 mM solution of tetramisole hydrochloride (Sigma-Aldrich) in M9 and mounted on 6% agarose pads on glass slides. Image processing was performed with Fiji software (http://imagej.nih.gov/ij; v.1.47b). Each experiment was repeated at least once.

GFP quantification. Fluorescence intensity in worm strains expressing GFP-reporter proteins was quantified using a Victor X4 plate reader (Perkin Elmer). The animals were prepared in the following way: 80 worms per condition (at the corresponding ages) were transferred into wells filled with M9 medium (20 worms per well of a black-walled 96-well plate). Each experiment was repeated at least twice.

MitoSox ROS quantification. MitoSox staining was performed as previously described[11]. In brief, a population of 100 worms was recovered in 1 ml M9 buffer, washed five times to remove residual bacteria, and resuspended in 200 μl 1:200 MitoSox (Life technologies) stock solution (initial stock solution was dissolved at 1 mM in DMSO). After 20 min of treatment, worms were washed five times in 1 ml M9 buffer to eliminate the MitoSox reagent, and then transferred to a black-walled 96-well plate for reading using a Victor X4 plate reader (Perkin Elmer).

Enzymatic assays in *C. elegans*. Worms were collected in M9 and washed eight times to remove all residual bacteria. After the last wash, the maximum possible amount of M9 was aspirated and the remaining worm pellet was snap-frozen in liquid nitrogen. Activity of QPRT was assessed as previously described[37]. In brief, we coupled the QPRT reaction to the conversion of the reaction product NAMN to NAD^+ with the help of the ancillary enzymes NadD and NadE, followed by a quantification of NAD^+ with fluorometric cycling assay (Extended Data Fig. 1c). The buffer of the assay mixture consisted of 30 mM potassium phosphate buffer, pH 7.0, 0.5 mM $MgCl_2$. ACMSD activity was assayed as previously described[21]. In brief, formation of ACMS was monitored at 360 nm, at 37 °C, in a pre-assay mixture consisting of 30 μM hydroxyanthranilic acid and an excess quantity of recombinant *Ralstonia metallidurans* 3-hydroxyanthranilic acid dioxygenase. After the reaction was complete, an appropriate aliquot of worm extract was added and ACMS consumption was calculated by the decrease in absorbance. The activity value was corrected for the spontaneous decrease in absorbance due to the non-enzymatic cyclization of ACMS to quinolinic acid. To this end, a control mixture containing all reagents except the extract (replaced by an equal volume of a BSA solution at the same concentration of the extract) was monitored in parallel.

Tryptophan supplementation experiments in *C. elegans*. L-tryptophan (Sigma-Aldrich) was dissolved in water to obtain a 50 mM solution. This freshly prepared solution was added into the NGM agar at the moment of plate preparation to obtain the concentrations stated in the main text. Worms were maintained on the tryptophan-supplemented plates seeded with live bacteria (*E.coli* OP50) through their larval stages to allow development. At L4 larvae stage, worms were collected in M9 solution, washed seven times to remove all the residual bacteria in their intestines and transferred to tryptophan-supplemented plates seeded with heat-inactivated bacteria (*E.coli* OP50) to avoid metabolism of L-tryptophan by the bacteria. A 500 ml culture of OP50 bacteria was incubated at 37 °C overnight; the bacteria were then centrifuged at 3,320*g* for 30 min at 4 °C and the resulting bacterial pellet was dissolved in 50 ml fresh LB medium. Subsequently, heat inactivation was performed by incubating the bacteria at 95 °C for 30 min.

NAD^+ measurements. NAD^+ was extracted using acidic extraction method and analysed by HPLC–mass spectrometry as previously described[38]. In brief, ~10 mg of frozen tissue samples were used for NAD^+ extraction in 10% perchloric acid and neutralized in 3 M K_2CO_3 on ice. After final centrifugation, the supernatant was filtered and the internal standard (NAD^+-C13) was added and loaded onto a column (150 Å, ~ 2.1 mm; Kinetex EVO C18, 100 Å). HPLC was run for 1 min at a flow rate of 300 ml/min with 100% buffer A (methanol/H_2O, 80/20% v/v). Then, a linear gradient to 100% buffer B (H_2O + 5mM ammonium acetate) was performed (at 1 to 6 min). Buffer B (100%) was maintained for 3 min (at 6 to 9 min), and then a linear gradient back to 100% buffer A (at 9 to 13 min) started. Buffer A was then maintained at 100% until the end (at 13 to 18 min). NAD^+ eluted as a sharp peak at 3.3 min and was quantified on the basis of the peak area ratio between NAD^+ and the internal standard and normalized to tissue weight and protein content.

Cell culture. The mouse hepatocytes cell line AML-12 (alpha mouse liver 12) was obtained from ATCC and grown at 37 °C in a humidified atmosphere of 5% CO2/95% air in Dulbecco's Modified Eagle Medium/Nutrient Mixture F-12 (DMEM/F-12) supplemented with 0.005 mg/ml insulin, 0.005 mg/ml transferrin, 5 ng/ml selenium, 40 ng/ml dexamethasone, 0.5 mM tryptophan and 1% gentamycin.

Proximal tubular cell line HK-2 (human kidney 2) was purchased from ATCC and grown at 37 °C in a humidified atmosphere of 5% CO2/95% air in normal DMEM medium (Gibco) including 10% FCS (Gibco), 10 units per ml penicillin, 0.5 mM tryptophan and HEPES for buffering. ACMSD inhibitor was initially diluted from powder in DMSO to the stock concentration of 1 mM. This stock was further diluted with water to 100 μM, which was used for the cell treatments.

All the cell lines purchased from ATCC have been authenticated by morphology, karyotyping and PCR-based approaches. All the used cell lines have been routinely checked in the laboratory for mycoplasma contamination with the MycoProbe detection kit (R&D systems). Only cells negative for mycoplasma contamination were used.

Primary hepatocytes culture. Primary hepatocytes were prepared from 8 to 12-week-old C57BL/6 or *Sirt1*$^{L2/L2}$ mice (males and females) by liberase perfusion method as previously described[39], with minor modifications. Isolated primary hepatocytes were plated with DMEM medium (Gibco) including 10% FCS (Gibco), 10 units per ml penicillin, 0.5 mM tryptophan and HEPES for buffering. After 6–8 h of attachment, this medium was replaced with medium containing either different concentrations of ACMSD inhibitor or the corresponding concentration of DMSO, or transduced with adenovirus encoding either control shRNA or shRNA against *Acmsd*. Primary hepatocytes extracted from *Sirt1*$^{L2/L2}$ mice were transduced either with adenovirus encoding CRE-recombinase (to generate *Sirt1* knockout) or GFP. Primary hepatocytes were collected 24 h later in the case of pharmacological treatment and 48 h after adenoviral transduction. When indicated, cell culture medium was supplemented with palmitate-BSA and/or oleate-BSA.

Genetic knockdown of *Acmsd*. Five different pairs of single-stranded DNA oligonucleotides were designed and tested for *Acmsd* knockdown. 'Top strand' oligonucleotides: 1) 5′-caccggaagctcttcagagtgatcccgaaggatcactctgaagagcttcc-3′, 2) 5′-caccggagatggagcgttgtgttaacgaattaacacaacgctccatctcc-3′, 3) 5′-caccgctattgacagatgtcataggcgaacctatggacatctgtcaatagc-3′, 4) 5′-caccggaagctgatagagtccatggcgaaccatggactctatcagcttcc -3′, 5) 5′-caccgcagagtttgatgaagaaacacgaatgtttcttcatcaaactctgc -3′. 'Bottom strand' oligonucleotides (respectively): 1) 5′-aaaaggaagctcttcagagtgatccttcgggatcactctgaagagcttcc-3′, 2) 5′-aaaaggagatggagcgttgtgttaattcgttaacacaacgctccatctcc-3′, 3) 5′-aaaagctattgacagatgtcataggttcgcctatgacatctgtcaatagc-3′, 4) 5′-aaaaggaagctgatagagtccatggttcgccatggactctatcagcttcc-3′, 5) 5′-aaaagcagagtttgatgaagaaacattcgtgtttcttcatcaaactctgc-3′. BLOCK-iT U6 RNAi Entry Vector Kit (Intvitrogen) was used for production of an entry clone. BLOCK-iT Adenoviral

RNAi Expression System (Invitrogen) was used subsequently to produce an adenoviral expression clone. The shRNA no. 3 showed the highest knockdown efficacy and was used for all the experiments in this manuscript.

Apoptosis assessment. Caspase 3/7 activities were measured with the Caspase-Glo assay (Promega) according to the manufacturer's instructions. HK-2 cells were plated at 5×10^3 cells/well in a white ViewPlate-384 microplate (PerkinElmer). The cells were treated with 50 μM cisplatin (Sigma Aldrich) for 16 h. ACMSD inhibitor was either added simultaneously with cisplatin or 1 h before cisplatin addition (preventive). The data were graphed considering the cisplatin treatment as 100% and the vehicle treatment as 0% of caspase activity. Apoptosis in primary hepatocytes was induced by exposing the cells to 0.75 mM palmitate for 36 h.

SOD2 activity assay. Primary hepatocytes, AML-12 cells or pieces of frozen liver were lysed in 20 mM HEPES buffer (Gibco), pH 7.2, containing 1 mM EGTA (Sigma-Aldrich), 210 mM mannitol (Sigma-Aldrich) and 70 mM sucrose (AMRESCO). Total protein concentration was determined using the Bradford assay (BioRad). SOD2 activity was determined at indicated times after ACMSD inhibitor treatment by the SOD Assay Kit (Cayman Chemical) according to the manufacturer's instructions. To specifically detect the SOD2 activity 2 mM potassium cyanide was added to the assay, which inhibited both Cu/Zn-SOD and extracellular SOD, resulting in the detection of only Mn-SOD (SOD2) activity. Absorbance was determined with a Victor X4 multilabel plate reader (Perkin-Elmer) at 450 nm. Results are expressed in U/ml/mg of protein according to the standard curve and measured protein concentration.

Oxygen consumption. Oxygen consumption was measured with the Seahorse XF96 instrument (Seahorse Bioscience) according to the manufacturer's protocol. FCCP at the indicated concentrations was used as an uncoupler to reach maximal respiration.

Fatty acid oxidation. Fatty acid oxidation was measured in primary mouse hepatocytes with the Seahorse XF96 instrument (Agilent Seahorse), following the manufacturer's protocol. This protocol quantified the oxidation of both exogenous and endogenous fatty acids. Cells were cultured in conditions that would stimulate the depletion of endogenous substrates to prime the cells for oxidation of exogenous fatty acids. Four different conditions were used for each of the treatment groups. These conditions included etomoxir+ palmitate−, etomoxir+ palmitate+, etomoxir− palmitate− and etomoxir− palmitate+. To determine endogenous fatty acid utilization etomoxir+ conditions were used, as cells treated with etomoxir were unable to import exogenous fatty acids into the mitochondria.

Steatosis assessment in cells. Extent of steatosis and triglyceride accumulation within cells were assessed with Steatosis Colorimetric Assay Kit (Cayman) and Triglyceride Colorimetric Assay Kit (Cayman), according to manufacturer's instructions. Triglycerides were normalized by protein content, which was determined using the Bradford assay (BioRad).

ROS quantification in cells. ROS levels were measured by staining cells with 20 μM 2′,7′-dichlorofluorescin (DCFDA) reagent (Abcam) for 45–60 min at 37 °C. The DCFDA solution was then removed and cells were washed twice with PBS. The quantification of the signal was performed with a Victor X4 multilabel plate reader (Perkin-Elmer) with maximum excitation and emission spectra of 495 nm and 529 nm, respectively.

RNA isolation and RT–PCR. Total RNA was extracted using TRIzol (Invitrogen), according to the manufacturer's instructions. RNA was treated with DNase, and 2 μg RNA was used for reverse transcription. cDNA diluted 15× or 20× was used for quantitative PCR with reverse transcription (RT–qPCR) reactions. The RT–qPCR reactions were performed using the Light-Cycler system (Roche Applied Science) and a qPCR Supermix (QIAGEN) with the indicated primers. The average of at least three technical repeats was used for each biological data point. The list of primers used and their sequences are available upon request. The experiments were repeated at least twice (starting from RNA isolation). In case of contradictions in the results between the two repetitions, the experiment was repeated for a third time.

Protein isolation and western blot. Proteins were extracted with RIPA buffer containing protease and phosphatase inhibitors and analysed by SDS–PAGE and western blot. Proteins were detected using the following specific antibodies: ACMSD (Abcam, ab96081), actin (Sigma, A5441), acetyl-FKHR (Santa Cruz, sc-49437), FOXO1 (Cell Signaling, 2880), HSP90 (BD Transduction Laboratories, 610418), Total OXPHOS Rodent Antibody Cocktail (Abcam, ab110413), tubulin (Santa Cruz, sc-5286), vinculin (Abcam, ab129002). All antibodies were validated by the manufacturer.

Mitochondrial isolation, blue native polyacrylamide gel electrophoresis and in-gel activity assays. Mitochondrial isolation was performed as previously described[40]. In brief, ∼30 mg of liver tissue or a pool of 10,000 worms was used for mitochondrial isolation. The samples were homogenized in ice-cold sucrose-containing isolation buffer with a glass/teflon Potter–Elvehjem homogenizer (Wheaton, cat. No. 358029) and mitochondria were pelleted through multiple rounds of centrifugation at different speeds. For blue native PAGE, 50 μg of mitochondria from liver was solubilized in digitonin and sample buffer (Invitrogen, BN2008). Electrophoresis was performed using Native PAGE Novex Bis-Tris Gel System (3 to 12%), as per manufacturer's instructions with minor modifications. Gel transfer was performed using Invitrogen iBlot gel transfer system. For detection of the complexes, anti-OXPHOS cocktail (Invitrogen, 457999) and WesternBreeze Chromogenic Western Blot Immunodetection Kit (Invitogen, WB7103) were used. In the final detection step, the membrane was incubated with the chromogenic substrate for 8 min for all the gels.

For in-gel activity assays, electrophoresis was performed for 3 h (30 min at 150 V and 2.5 h at 250 V). Complex I activity was performed by incubating the gels for 15 to 30 min in the substrate composed of 2 mM tris-HCl pH 7.4; 0.1 mg/ml NADH, and 2.5 mg/ml nitrotetrazolium blue. Complex IV activity was performed by incubating the gels for 30 to 40 min in the substrate composed of 25 mg of 3,3′-diamidobenzidine tetrahydrochloride; 50 mg cytochrome *c*; 45 ml 50 mM phosphate buffer pH 7.4, and 5 ml water. Complex IV + complex I activity was performed by subsequently incubating the gels in the substrate for CIV followed by incubation in complex I substrate. Complex II activity was checked on a separate gel, which was incubated in the substrate composed of 20 mM sodium succinate, 2.5 mg/ml nitrotetrazolium blue, 0.2 mM phenazine methosulfate and 5 mM tris-HCl buffer. All reactions were stopped with 10% acetic acid.

SIRT1 activity. SIRT1 activity was assessed with SIRT1 Direct Fluorescent Screening Assay Kit (Cayman Chemical), according to the manufacturer's instructions. The absorbance was read at 450 nm.

mtDNA copy number. Mitochondrial number was assessed by using mtDNA: nDNA ratio. mtDNA was quantified as previously described[41], with slight modifications. In brief, total DNA was extracted with the Nucleospin Tissue Kit (Macherey Nagel). Forty nanograms total DNA was assessed by real-time PCR using a Light Cycler 480 (Roche). The reaction was performed in a final volume of 8 μl with 1× SYBR green master mix (Roche) and 1.25 μM of the reverse and forward primers. UCP2 primers were used as endogenous control for nDNA and 16S as marker for mtDNA.

Statistics. No statistical methods were used to predetermine sample size. Survival analyses were performed using the Kaplan–Meier method and the significance of differences between survival curves calculated using the log-rank test. Differences between two groups were assessed using two-tailed *t*-tests. To compare the interaction between age and genotype, two-way ANOVA tests were performed. Analysis of variance, assessed by Tukey's or Dunnett's multiple comparison test, was used when comparing more than two groups. We used GraphPad Prism 6 (GraphPad Software) for all other statistical analyses. Sample sizes were chosen without performing statistical tests, but based on studies with similar experimental design and on the known variability of the assay. All *P* values <0.05 were considered significant. $*P<0.05$; $**P\leq 0.01$; $***P\leq 0.001$ unless stated otherwise.

Mouse experiments. Mice were maintained in a controlled environment with 22 °C temperature, 50% humidity, 15–20 fresh air changes per hour and light–dark cycle of 12 h. They were housed 3–4 animals per cage with ad libitum access to fresh water and food and with appropriate environmental enrichment within the cage. All animal experiments were performed according to Swiss ethical guidelines and approved by the Service de la Consommation et des Affaires Vétérinaires (SCAV) of the Canton de Vaud. Animals that showed signs of severity, predefined by the animal authorizations, were euthanized and removed from the calculations. All experiments on mice were done in a non-blinded way.

Generation of *Sirt1*$^{hep-/-}$ mice. Liver-specific *Sirt1* knockout (*Sirt1*$^{hep-/-}$) mice were generated as previously described[29], by breeding *Sirt1*$^{L2/L2}$ mice[11] with Alb-Cre mice, which express Cre recombinase under the control of the albumin promoter.

MCD diet-induced NAFLD. Twelve-week-old, C57BL/6J male mice were acclimatized for a period of seven days before initiation of the experiment. After the acclimatization period the mice were randomized based on their body weight and separated into three groups: one group received methionine-choline deficient (MCD) diet (Harlan Teklad TD.90262) containing vehicle (DMSO 5% + polyethylene glycol (PEG) 20%), the second received MCD diet supplemented with 15 mg kg^{-1} body weight day^{-1} ACMSD inhibitor (TES-991) and the third receiving the matched control diet (Harlan Teklad TF.94149) with the vehicle (DMSO 5% + PEG 20%). Two and a half weeks after the beginning of the special diets, animals fasted for 4 h were subjected to isoflurane anaesthesia and blood was sampled via cardiac puncture. Plasma was collected by centrifugation at 4,000 r.p.m. for 10 min at 4 °C. Collected tissues and plasma were snap-frozen in liquid nitrogen. The experiment was performed once.

Histopathology on MCD diet liver tissues. A piece of liver tissue (always from the same lobe) was fixed with 10% neutral buffered formaldehyde, processed and embedded in paraffin. After sectioning, tissue was stained with H&E. Another liver piece (always from the same lobe) was embedded in Shandon Cryomatrix resin (Thermo Scientific Scientific) and snap-frozen in isopentane cooled in

liquid nitrogen, before being placed on dry ice. Oil red O and CD45 stainings were performed on cryosections as previously described[29].

Hepatic triglyceride content measurement. Hepatic lipids were extracted as previously described[42]. Triglyceride content in hepatic lipid fraction was quantified with enzymatic assays (Roche).

Ischaemia-reperfusion-induced AKI. Nine-week-old C57BL/6J males were acclimatized for seven days before initiation of the experiment. After the acclimatization period, the mice were randomized based on their body weight and separated into three groups: two groups received normal chow diet (Harlan Teklad 2916) containing vehicle (DMSO 5% + polyethylene glycol (PEG) 20%), the third group received normal chow diet supplemented with 15 mg kg^{-1} body weight day^{-1} ACMSD inhibitor (TES-1025). On day 10 after the beginning of the diet, mice were anaesthetized with isoflurane and placed on a surgical platform in a dorsal position. Both kidneys were exposed through flank incisions and renal pedicles were occluded using vascular clamps for 25 min. The clamp was then removed and the surgical site was sutured. Physiological saline (1 ml) was administered intraperitoneally after closing the wound to prevent dehydration. The sham-operated group was subjected to similar surgical procedures, except that the occluding clamp was not applied. A suitable analgesic (Dafalgan) was administered post-operatively to all animals. Animals were monitored for recovery from anaesthesia and then housed singly in their home cage with appropriate environmental enrichment. Forty-eight hours after the surgery, animals were subjected to isoflurane anaesthesia and blood was sampled by cardiac puncture, followed by organ collection. Plasma was collected by centrifugation at 4,000 r.p.m. for 10 min at 4 °C. Plasma was separated into a fresh tube and stored at −80 °C. Collected tissues were snap-frozen in liquid nitrogen. The experiment was performed once.

Cisplatin-induced AKI. Eight-week-old C57BL/6J males were acclimatized for 5–7 days before initiation of the experiment. Animals were randomized into different treatment groups based on their body weight and BUN levels. After randomization the groups were maintained on specified diet, either normal chow diet (Teklad global 16% protein rodent diet; Harlan Laboratories 2016S) or chow diet supplemented with ACMSD inhibitor, for 10 days. Body weight and food consumption were monitored during this period. Cisplatin was injected intraperitoneally with 1 ml syringe with 26G needle at a dose of 20 mg/kg of body weight. The sham control group was administered with the same volume of 0.9% saline. Animals were monitored every day for body-weight loss, general health conditions and signs of pain, distress and mortality. Seventy-two hours after cisplatin injection animals were subjected to isoflurane anaesthesia and blood was sampled by cardiac puncture, followed by organ collection. Plasma was collected by centrifugation at 4,000 r.p.m. for 10 min at 4 °C. Plasma was separated into a fresh tube and stored at −80 °C. Collected tissues were snap-frozen in liquid nitrogen. The experiment was performed twice.

Glomerular filtration rate measurement. Determination of glomerular function rate was performed in conscious mice using transcutaneous measurement of FITC-sinistrin (Mannheim Pharma and Diagnostic) elimination as previously described[43,44], using miniaturized devices containing an optical component and a microprocessor (Medibeacon). In brief, 55 h post-cisplatin administration, mice were subjected to a light (1.5–2% isoflurane) anaesthesia to affix the device and a rechargeable battery on a depilated region of the back using a double-sided sticky patch. The device was further held in place with a piece of Transpore tape (3M) surrounding the animal body. After a resting period of 2–5 min, a bolus of FITC-sinistrin (35 mg per 100 g, dissolved in saline) was injected through the tail vein. The excretion kinetics of FITC-sinistrin was recorded in conscious animals for an average of 60 min as a decay of subcutaneous fluorescence of FITC-sinistrin. Elimination half-life ($t_{1/2}$) was determined from the single exponential phase of the excretion curve and then converted to GFR using a semi-empirical conversion factor developed and validated for mice as previously described[44].

Histopathology on AKI kidneys. Half of a kidney was fixed with 10% neutral-buffered formaldehyde, processed and embedded in paraffin. After sectioning, tissue was stained with H&E. Histopathological scoring was performed by two different pathologists in a blinded and independent way. The scoring system was adapted from ref.[45] with slight modifications. Tubular cell necrosis, tubular dilatation, inflammatory cell infiltration, oedema and cast formation were scored.

Quantification of intermediates in tryptophan pathway. Snap-frozen brain, liver and kidney samples were ground into powder with liquid nitrogen, using a mortar and pestle. Each sample was then pre-weighed (~50 mg) into lysis tubes (soft tissue homogenizing CK 14 tubes) and stored at −80 °C before metabolite extraction. Frozen tissue powders were extracted by the addition of an ice-cold methanol–H_2O 4:1 mixture (100 µl for every 10 mg of tissue) and homogenized using ceramic beads in the Cryolys Precellys 24-sample Homogenizer (2 × 20 s at 10,000 r.p.m.; Bertin Technologies), which was air-cooled by a flow rate at 110 l/min at 6 bar. Homogenized extracts were centrifuged for 15 min at 4,000*g* at 4 °C and the supernatant (tissue extract) was removed and used in further preparation for liquid chromatography–tandem mass spectrometry (LC–MS/MS) analysis.

For the analysis of tryptophan pathway intermediates and NAD^+, in negative ionization mode, the sample was prepared by mixing an aliquot of tissue extract (50 µl) with 250 µl of the ice-cold internal standard solution (in 100% acetonitrile). For the analysis of end products of kynurenine pathway (that is, picolinic, quinolinic and nicotinic acid), in positive ionization mode, 300 µl of the tissue extract was evaporated to dryness (using a CentriVap vacuum concentrator, LabConco), and reconstituted with 75 µl 0.2% formic acid in H_2O. Samples were centrifuged and supernatant was injected for LC–MS/MS analysis.

LC–MS/MS analyses were performed using a 6495 triple quadrupole mass spectrometer (QqQ) interfaced with a 1290 UHPLC system (Agilent Technologies) and operated in the dynamic Multiple Reaction Monitoring (dMRM) mode.

Quinolinic, picolinic and nicotinic acid were measured in positive electrospray ionization (ESI + MS) mode, using an Acquity HSS T3 column (2.1 × 100 mm, 1.8 µm, Waters). An 11-min gradient was applied starting at 0% B (0.2% formic acid in methanol, 0–2 min) and increasing to 50% (2–4 min), and further to 90% (4–5 min), before returning to starting conditions (5–7 min) and re-equilibrating for 4 min (7–11 min). Mobile phase A was 0.2% formic acid in H_2O, the flow rate for this method was 400 µl/min and the sample injection volume was 5 µl. ESI source conditions were set as follows: dry gas temperature 250 °C, nebulizer 35 psi and flow 15 l/min, sheath gas temperature 250 °C and flow 8 l/min, nozzle voltage 1,000 V, and capillary voltage +3,000 V. The cycle time in dMRM mode was 500 ms. Standard calibration curves ranging from 0–50 µM were used for quantification for all three organic acids.

NAD^+ was measured in negative electrospray ionization (ESI-MS) mode, using a SeQuant ZIC-pHILIC column (10 × 2.1 mm internal diameter, 5 µm) with a SeQuant ZIC-pHILIC guard column (20 × 2.1 mm internal diameter, 5 µm (Merck)) at an operation temperature of 30 °C. Mobile phase A was composed of 20 mM ammonium acetate and 20 mM ammonium hydroxide in H_2O (pH 9.3) and mobile phase B was 100% acetonitrile, and the sample injection volume was 2 µl. The linear gradient elution started at 90% B (0–1.5 min), decreased to 50% B (8–11 min), decreased further to 45% B (12–15 min), restored to 90% (15–16 min) and subsequently re-equilibrated for 9 min at a flow rate of 300 µl/min. ESI source conditions were set as follows: dry gas temperature 290 °C, nebulizer 35 psi and flow 14 l/min, sheath gas temperature 350 °C and flow 12 l/min, nozzle voltage 0 V, and capillary voltage −2,000 V. Cycle time in dMRM mode was 600 ms. The following calibration curve range was used for NAD^+ quantification: 0–316 µM. NAD^+ concentrations were reported with an external calibration curve only (IS not available). Collision energies and product ions (MS2 or quantifier and qualifier ion transitions) were pre-optimized for each metabolite of interest.

Data processing, including the peak integration and concentration calculation was performed in Masshunter Quantitative Analysis (for QqQ, v.B.07.01/ Build 7.1.524.0, Agilent Technologies). Linearity of the standard curves was evaluated for each metabolite using a 6-point range; in addition, peak area integration was manually curated and corrected where necessary. Concentrations of the compounds for which the IS were available were corrected for the ratio of MS response (peak area) between the analyte and the IS, to account for matrix effects.

Glutathione assay. Glutathione quantities in the kidney were assayed using the ELISA kit (Cayman Chemicals) according to the manufacturer instructions.

Myeloperoxidase assay. Myeloperoxidase (MPO) in kidney tissue was quantified by ELISA kit (Abcam) according to the manufacturer instructions.

Reporting summary. Further information on research design is available in the Nature Research Reporting Summary linked to this paper.

Data availability

The authors declare that all the data supporting the findings of this study are available from the corresponding author upon request.

34. Kamath, R. S., Martinez-Campos, M., Zipperlen, P., Fraser, A. G. & Ahringer, J. Effectiveness of specific RNA-mediated interference through ingested double-stranded RNA in *Caenorhabditis elegans*. *Genome Biol.* **12**, RESEARCH0002 (2001).
35. Mouchiroud, L. et al. Pyruvate imbalance mediates metabolic reprogramming and mimics lifespan extension by dietary restriction in *Caenorhabditis elegans*. *Aging Cell* **10**, 39–54 (2011).
36. Mouchiroud, L. et al. The Movement Tracker: a flexible system for automated movement analysis in invertebrate model organisms. *Curr. Protoc. Neurosci.* **77**, 8.37.1–8.37.21 (2016).
37. Zamporlini, F. et al. Novel assay for simultaneous measurement of pyridine mononucleotides synthesizing activities allows dissection of the NAD^+ biosynthetic machinery in mammalian cells. *FEBS J.* **281**, 5104–5119 (2014).
38. Yang, T. & Sauve, A. A. NAD metabolism and sirtuins: metabolic regulation of protein deacetylation in stress and toxicity. *AAPS J.* **8**, E632–E643 (2006).
39. Oosterveer, M. H. et al. LRH-1-dependent glucose sensing determines intermediary metabolism in liver. *J. Clin. Invest.* **122**, 2817–2826 (2012).

40. Jha, P., Wang, X. & Auwerx, J. Analysis of mitochondrial respiratory chain supercomplexes using blue native polyacrylamide gel electrophoresis (BN-PAGE). *Curr. Protoc. Mouse Biol.* **6**, 1–14 (2016).
41. Lagouge, M. et al. Resveratrol improves mitochondrial function and protects against metabolic disease by activating SIRT1 and PGC-1α. *Cell* **127**, 1109–1122 (2006).
42. Jha, P. et al. Role of adipose tissue in methionine-choline-deficient model of non-alcoholic steatohepatitis (NASH). *Biochim. Biophys. Acta* **1842**, 959–970 (2014).
43. Schock-Kusch, D. et al. Transcutaneous measurement of glomerular filtration rate using FITC-sinistrin in rats. *Nephrol. Dial. Transplant.* **24**, 2997–3001 (2009).
44. Schreiber, A. et al. Transcutaneous measurement of renal function in conscious mice. *Am. J. Physiol. Renal Physiol.* **303**, F783–F788 (2012).
45. Melnikov, V. Y. et al. Neutrophil-independent mechanisms of caspase-1- and IL-18-mediated ischemic acute tubular necrosis in mice. *J. Clin. Invest.* **110**, 1083–1091 (2002).

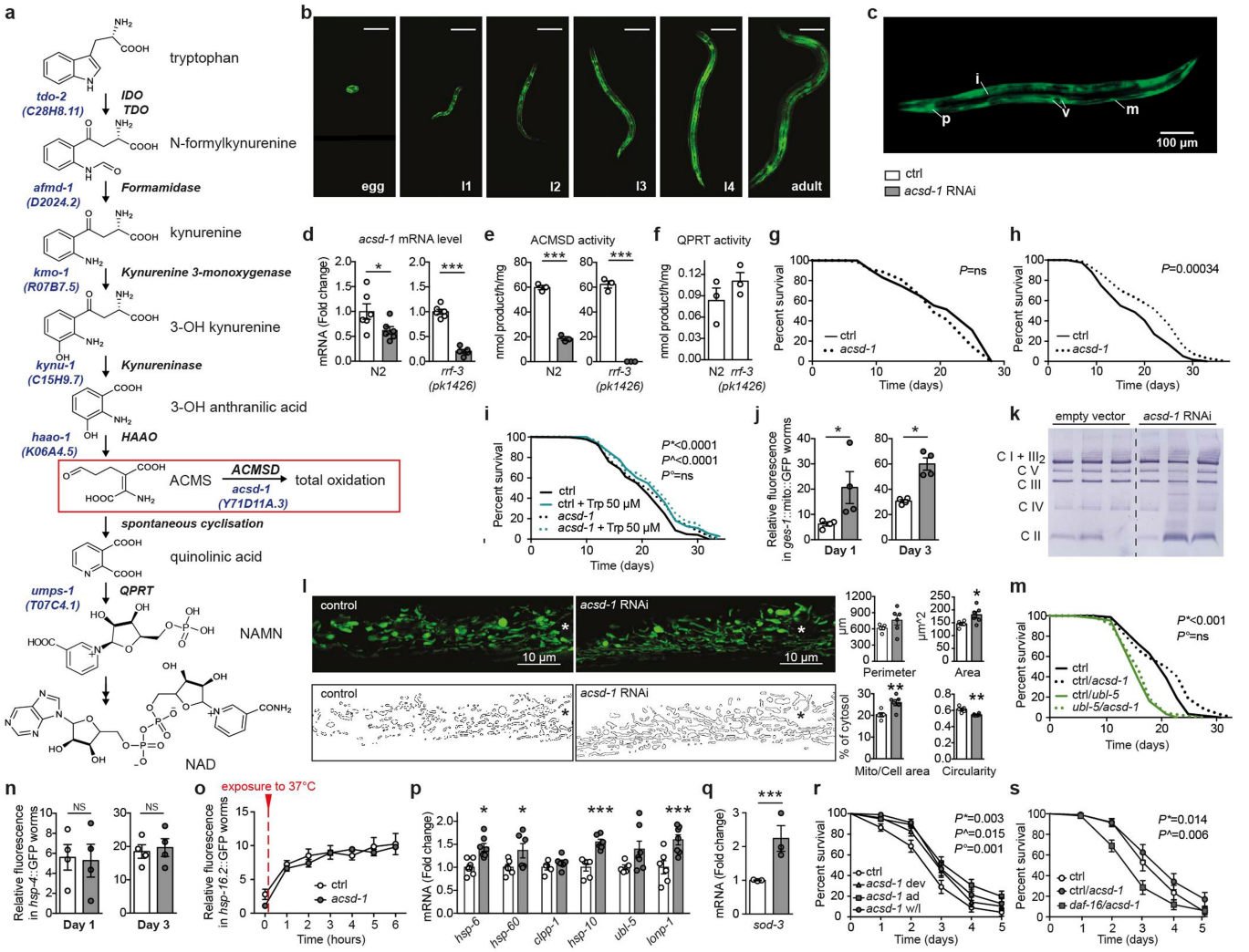

Extended Data Fig. 1 | *acsd-1* LOF improves NAD$^+$ levels, mitochondrial function, and lifespan through de novo synthesis in *C. elegans*. **a**, De novo synthesis of NAD$^+$ from tryptophan. Names of the worm's orthologues are in blue. **b**, *acsd-1* expression pattern across different developmental stages in wild-type worms expressing extrachromosomal array of *acsd-1*::GFP transgene. Scale bar, 100 µm. **c**, *acsd-1* expression pattern in adult wild-type worms expressing extrachromosomal array of *acsd-1*::GFP transgene. i, intestine; m, muscle; p, pharynx; v, vulva. **d**, *acsd-1* mRNA levels in wild-type and *rrf-3(pk1426)* mutants ($n = 6$, each n represents a pool of ~600 worms). **e**, ACSD-1 activity in control (empty vector) versus *acsd-1* RNAi-fed worms quantified in both wild-type and *rrf-3* mutants ($n = 3$, where each n represents a pool of ~3,600 worms) with compensation for negative controls. **f**, QPRT-like activity can be detected in both wild-type worms and *rrf-3* mutants ($n = 3$, each n represents a pool of ~3,600 worms). **g**, **h**, Effects of *acsd-1* knockdown throughout the entire life on N2 (**g**) and *rrf-3* mutant (**h**) worm lifespan. **i**, Lifespan of *rrf-3(pk1426)* mutants exposed to control or *acsd-1* RNAi upon tryptophan supplementation. *P**, ctrl versus ctrl + Trp 50 µM; *P*^, ctrl versus *acsd-1* RNAi; *P*°, ctrl + Trp 50 µM versus *acsd-1* RNAi + Trp 50 µM. **j**, Quantification of GFP signal in *ges-1*::mito::GFP reporter strain, expressing mitochondria-targeted GFP in the intestine at day 1 and 3 of adulthood ($n = 4$, each n represents a pool of 20 worms). **k**, Blue native PAGE on mitochondria extracted from *rrf-3* mutant worms fed with either empty vector or *acsd-1* RNAi bacteria at day 2 of adulthood ($n = 3$, each n represents mitochondria extracted from a pool of ~10,000 worms). **l**, Mitochondrial morphology in the P*myo-3*::mito::GFP reporter strain fed with control or *acsd-1* RNAi. Stars represent nuclei. Scoring includes the total perimeter of the mitochondrial network, its total area, the area occupied by the mitochondria within the cell and the circularity assessment, in which 1 is a perfect circle and 0 is a line ($n = 6$ worms). **m**, Epistasis between RNAi for *acsd-1* and the UPR^{mt} regulator, *ubl-5*. *P**, ctrl versus ctrl/*acsd-1* RNAi; *P*°, ctrl/*ubl-5* RNAi versus *ubl-5*/*acsd-1* RNAi. **n**, Quantification of the GFP signal in *hsp-4*::GFP reporter strain ($n = 4$, each n represents a pool of 20 worms) at day 1 and 3 of adulthood. **o**, Quantification of the GFP signal in *hsp-16.2*::GFP reporter strain ($n = 4$, each n represents a pool of 20 worms). After the first time point sampled at 20 °C, worms were exposed to 37 °C, and the measurement was repeated every hour for 6 h. **p**, Expression of UPR^{mt} genes in worms at day 2 of adulthood fed with control or *acsd-1* RNAi ($n = 6$, each n represents a pool of ~600 worms). **q**, Expression of *sod-3* mRNA at day 1 of adulthood in control or *acsd-1* RNAi-fed worms ($n = 3$, each n represents a pool of ~600 worms). **r**, Survival of wild-type (N2) worms exposed to 4 mM paraquat starting at the L4 stage, in which the knockdown of *acsd-1* was performed at different life stages. *P**, ctrl versus *acsd-1* RNAi whole life; *P*^, ctrl versus *acsd-1* RNAi development; *P*°, ctrl versus *acsd-1* RNAi adulthood. **s**, Epistasis between RNAi for *acsd-1* and *daf-16* in wild-type (N2) worms exposed to 4 mM paraquat. *P**, ctrl versus ctrl/*acsd-1* RNAi; *P*^, ctrl/*daf-16* RNAi versus *daf-16*/*acsd-1* RNAi. All worm assays, except for *hsp-16.2*::GFP reporter strain, were performed at 20 °C and repeated at least once. Data are mean ± s.e.m. $*P \leq 0.05$, $**P \leq 0.01$, $***P \leq 0.001$. *P* values calculated using two-tailed *t*-test (**d**, **e**, **j**, **l**, **n**–**q**) or log-rank test (**g**–**i**, **m**, **r**, **s**). For individual *P* values, see Source Data. For lifespan values, see Extended Data Table 1.

a

Cell type	C_t
HepG2	37.4 ± 0.9
HuH-7	28.8 ± 0.5
AML12	34.2 ± 0.8
HEK 293	ND
Hepa 1-6	35.0 ± 1.1
Mouse Primary Hepatocytes	27.2 ± 0.4
HK-2	28.5 ± 0.8

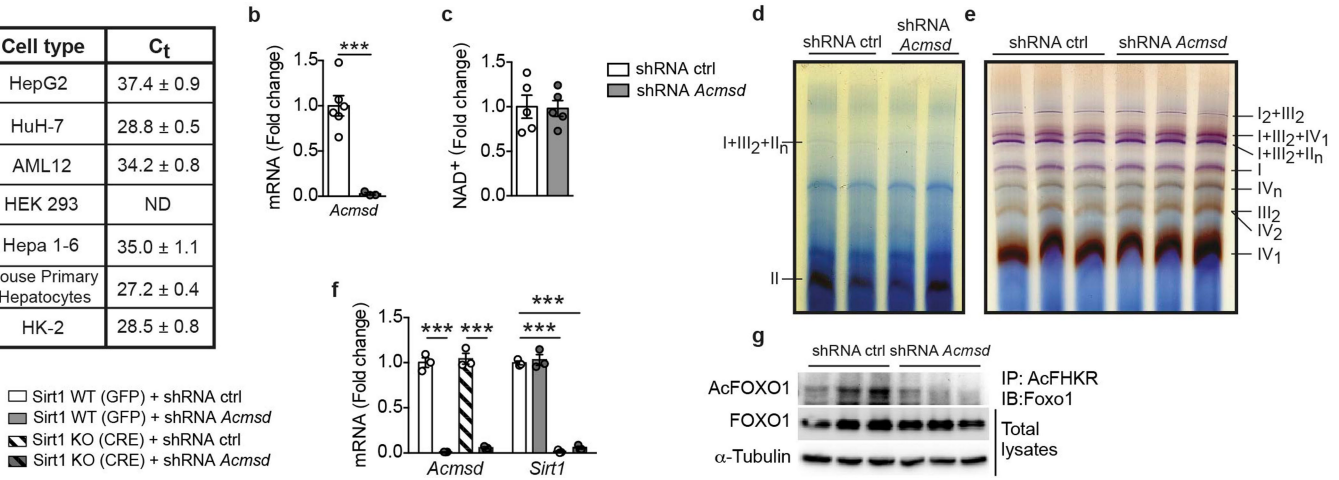

Extended Data Fig. 2 | Pathways activated by *Acmsd* knockdown in worms are conserved in mammalian cells. a, *Acmsd* transcript levels reflected by the C_t values in different hepatic and renal cells and cell lines ($n = 4$). C_t values larger than 35 reflect very low transcript levels. **b**, Efficiency of *Acmsd* shRNA in mouse primary hepatocytes 48 h post adenoviral transduction ($n = 6$). **c**, NAD^+ levels in mitochondria of AML-12 cells transduced with either shRNA control or shRNA against *Acmsd* ($n = 5$). **d**, **e**, Blue native PAGE followed by in-gel activity assay for complex II (blue) (**d**), and complex I (purple) and IV (brown) (**e**) on mitochondria extracted from mouse primary hepatocytes transduced with either shRNA control or shRNA against *Acmsd* for 48 h. The experiment was performed once. **f**, Primary hepatocytes extracted from a *Sirt1*$^{L2/L2}$ mouse were transduced either with an adenovirus encoding GFP (wild-type condition) or the Cre recombinase to generate *Sirt1* knockout primary hepatocytes. These hepatocytes were exposed to an shRNA targeting a random sequence or shRNA targeting *Acmsd*. Transcript levels of *Acmsd* and *Sirt1* ($n = 3$). **g**, FOXO1 acetylation levels in mouse primary hepatocytes transduced with either shRNA control or shRNA against *Acmsd* for 48 h. The experiment was independently performed twice. Data are mean ± s.e.m.; each *n* represents a biologically independent sample. $^*P \leq 0.05$, $^{**}P \leq 0.01$, $^{***}P \leq 0.001$. *P* values calculated using two-tailed *t*-test. For gel source images see Supplementary Fig. 1. For individual *P* values, see Source Data.

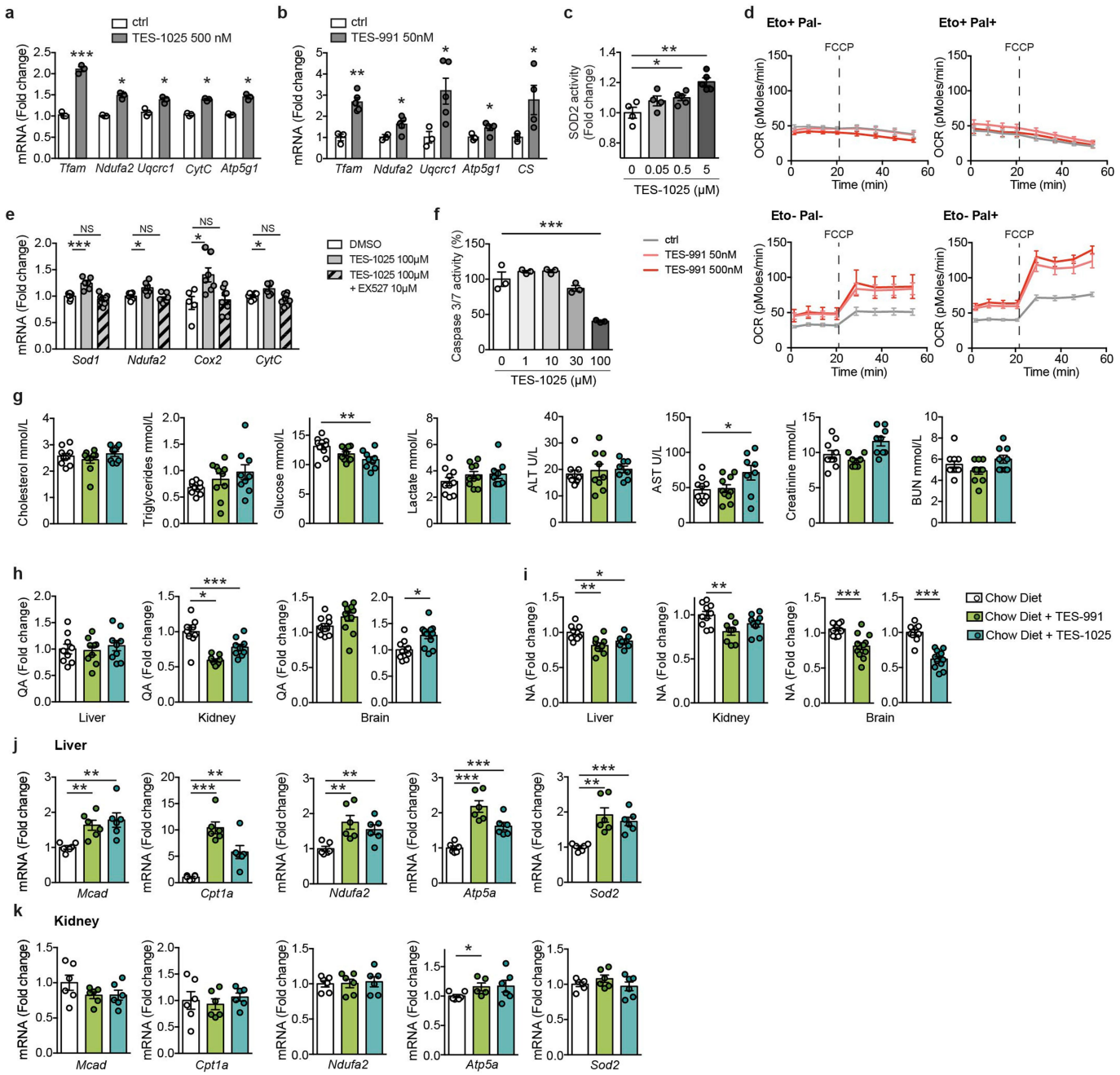

Extended Data Fig. 3 | Pharmacological inhibition of ACMSD has similar effects to genetic downregulation. a, **b**, mRNA levels of mitochondrial genes in mouse primary hepatocytes treated for 24 h with DMSO or TES-1025 (**a**) or TES-991 (**b**), at the indicated concentrations ($n = 3$). **c**, SOD2 activity in mouse primary hepatocytes treated for 24 h with DMSO or TES-1025, at indicated concentrations ($n = 4$). **d**, Fatty acid oxidation assessed in mouse primary hepatocytes treated with DMSO or TES-991 for 24 h at the indicated concentrations ($n = 5$). FCCP (2 μM) was used as an uncoupler to reach maximal respiration. **e**, mRNA levels of mitochondrial genes in HK-2 cells after 24 h of treatment with TES-1025 or TES-1025 in combination with SIRT1 inhibitor, EX527, at the indicated concentrations ($n = 5$–8). **f**, Apoptosis rate in HK-2 cells assessed 16 h after addition of 50 μM cisplatin by caspase-3/7 activity. TES-1025 was added simultaneously with the cisplatin. **g**, Biochemical analysis of plasma from mice fed with chow diet or chow diet supplemented with TES-991 or TES-1025 at 15 mg kg^{-1} body weight day^{-1} (ctrl and TES-991, $n = 10$; TES-1025, $n = 9$ mice). **h**, **i**, Quinolinic acid (QA) (**h**) and nicotinic acid (NA) (**i**) levels in livers ($n = 9$), kidneys (ctrl, $n = 10$; TES-991, TES-1025, $n = 9$ mice) and brains (ctrl, $n = 11$; TES-991, TES-1025, $n = 12$ mice), from mice fed with control chow diet or chow diet supplemented with TES-991 or TES-1025 at the dose of 15 mg kg^{-1} body weight day^{-1}. **j**, **k**, mRNA levels of β-oxidation, mitochondrial and oxidative stress defence genes in livers (**j**) and kidneys (**k**) of mice described in **g** ($n = 6$ mice). Data are mean ± s.e.m. $^*P \leq 0.05$, $^{**}P \leq 0.01$, $^{***}P \leq 0.001$. *P* values calculated using two-tailed *t*-test (**a**–**d**, **g**–**k**) or one-way ANOVA (**e**, **f**). For individual *P* values, see Source Data.

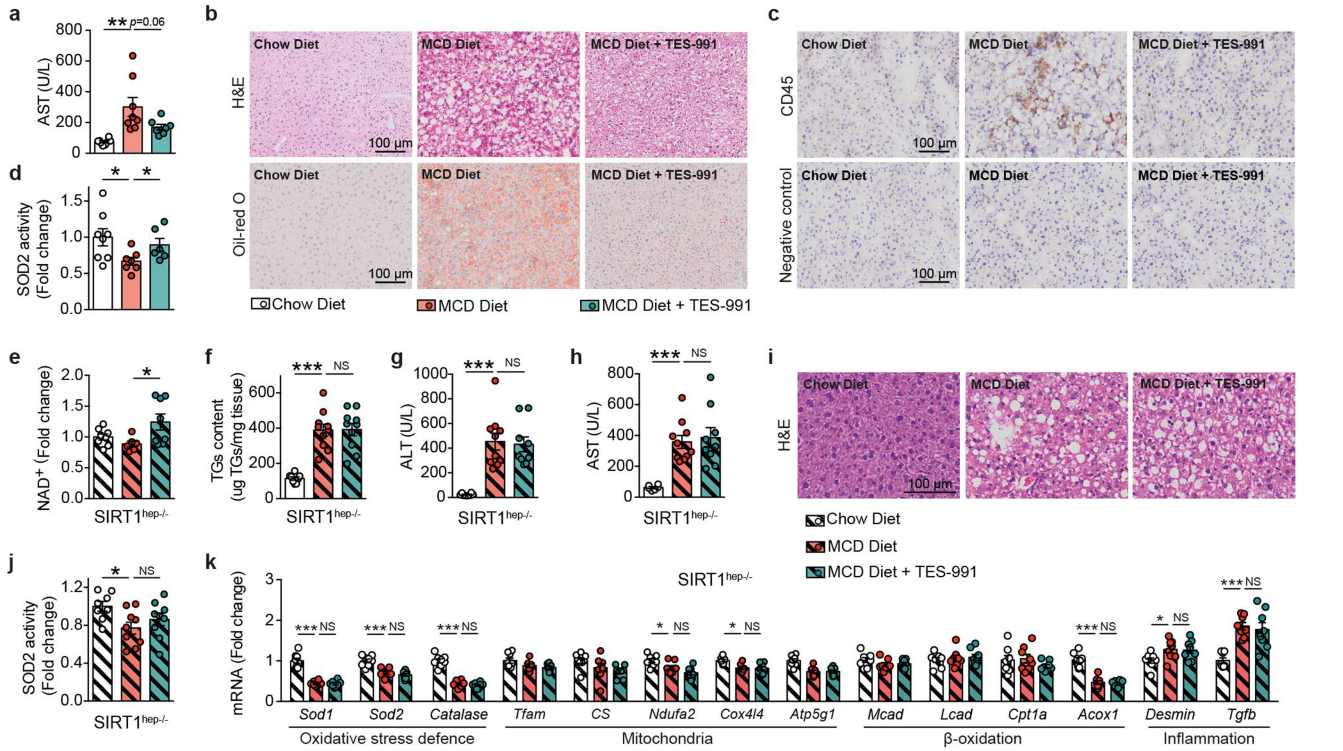

Extended Data Fig. 4 | ACMSD inhibitors protect hepatic function from NAFLD induced by MCD diet. a, Plasma aspartate transaminase (AST) levels in 16-week-old C57BL/6J male mice fed for 2.5 weeks with control diet, MCD diet or MCD diet supplemented with 15mg kg^{-1} day^{-1} TES-991 ($n = 8$ mice). **b**, Representative photomicrographs of liver tissues stained with H&E or Oil red O from the mouse cohorts described in **a**. The experiment was performed twice independently. **c**, Representative photomicrographs of liver tissues from the mouse cohorts described in **a**, stained with CD45 and the corresponding negative control. The experiment was performed twice independently. **d**, Hepatic SOD2 activity in mouse cohorts described in **a** (chow diet, $n = 8$; MCD diet, $n = 7$; MCD diet + TES-991, $n = 6$ mice). **e**–**h**, Liver NAD^+ (**e**), triglyceride content (**f**), plasma ALT (**g**) and AST (**h**) levels in congenic C57BL/6J $Sirt1^{hep-/-}$ mice that match the mouse cohorts described in **a** regarding age, gender and treatment duration (chow diet, $n = 8$; MCD diet, MCD diet + TES-991, $n = 10$ mice). **i**, Representative photomicrographs of liver tissues stained with H&E from the $Sirt1^{hep-/-}$ mice described in **e**–**h**. The experiment was performed once. **j**, Hepatic SOD2 activity in congenic C57BL/6J $Sirt1^{hep-/-}$ mice described in **e**–**h** (chow diet, $n = 8$; MCD diet, MCD diet + TES-991, $n = 9$ mice). **k**, mRNA levels of oxidative stress defence, mitochondrial, β-oxidation, inflammatory and fibrosis genes in livers of $Sirt1^{hep-/-}$ mice ($n = 8$ mice). Data are mean ± s.e.m. $*P \leq 0.05$, $**P \leq 0.01$, $***P \leq 0.001$. P values calculated using two-tailed t-test. For individual P values, see Source Data.

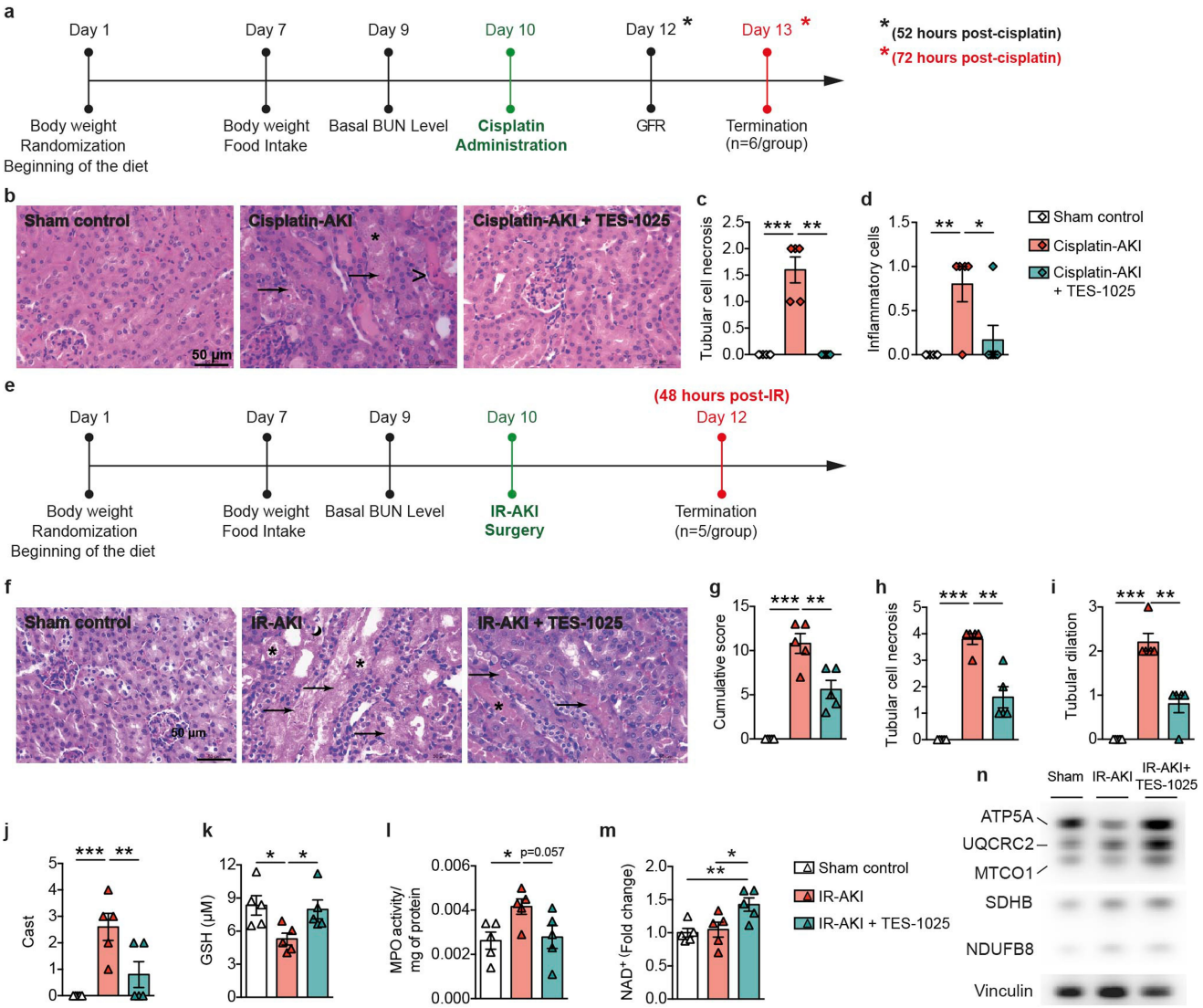

Extended Data Fig. 5 | ACMSD inhibitors protect renal function in two different models of AKI. a, Schematic timeline of the cisplatin-induced AKI study. AKI was induced at day 10 after the beginning of the study in male C57BL/6J mice by a single intraperitoneal dose of cisplatin (20 mg kg^{-1} body weight). Mice in the sham control group were injected with a saline solution. GFR was measured non-invasively 52 h post-cisplatin administration. **b**–**d**, Representative photomicrographs of H&E-stained kidney sections (**b**), histopathological scoring for tubular necrosis (**c**) and inflammatory cell infiltration (**d**) of mouse cohorts described in **a** (sham control, cisplatin-AKI + TES-1025, $n = 6$; cisplatin-AKI, $n = 5$ mice). **e**, Schematic timeline of the IR-AKI study. AKI was induced at day 10 after the beginning of the study in anaesthetized male C57BL/6J mice by a dorsal surgical incision and bilateral occlusion of the renal pedicles for 25 min. Mice in the sham control group underwent the same surgical procedure without application of the occluding clamp on the renal pedicles. **f**–**j**, Representative photomicrographs of H&E-stained kidney sections (**f**) and histopathological scoring for cumulative score (**g**), tubular necrosis (**h**), tubular dilation (**i**), and cast formation (**j**) of mouse cohorts described in **e** ($n = 5$ mice). Tubular cell necrosis (arrows), tubular dilation and casts (asterisk) and interstitial oedema (crescent moon) are indicated on the pictures. **k**–**m**, Glutathione protein levels (**k**), MPO activity (**l**) and NAD^+ content (**m**) in kidneys of the IR-AKI cohorts described in **e** ($n = 5$ mice). **n**, Protein expression of the respiratory complex subunits in kidneys from the mouse cohorts described in **e**. The experiment was performed independently twice. Data are mean ± s.e.m. $*P \leq 0.05$, $**P \leq 0.01$, $***P \leq 0.001$. *P* values calculated using two-tailed *t*-test. For gel source images see Supplementary Fig. 1. For individual *P* values, see Source Data. The histopathological scoring was performed independently by two pathologists in a blinded manner (**b**–**d**, **f**–**j**).

Extended Data Table 1 | Summary of *C. elegans* lifespan experiments

Conditions		Cumulative statistics					Statistics of individual exprts			
Strain	Treatment/RNAi	No. of expts.	Mean lifespan [days] (treatment/ctrl)	variation [%] compared to control	P-value	No. of animals (treatment/ctrl)	Mean lifespan [days] (treatment/ctrl)	variation [%] compared to control	P-value	No. of animals (treatment/ctrl)
N2	*acsd-1*	2	20.5/20.5 (±0.47/0.41)	0	0.3	116/124	20.2/20.9	-3.35	0.303	43/44
							20.6/20.2	+1.98	0.582	73/80
rrf-3 (pk1426)	*acsd-1*	2	21.4/18.5 (±0.56/0.56)	+15.7	0.00034	137/118	22.0/18.6	+18.3	0.004	70/66
							20.9/18.4	+13.6	0.042	67/52
rrf-3 (pk1426)	*acsd-1 1/2*	4	20.2/18.5 (±0.35/0.32)	+9.2	<0.0001	262/246	18.6/17.0	+9.4	0.047	61/57
							19.6/17.6	+11.4	0.03	59/64
							20.2/18.2	+11.0	0.009	63/61
							21.4/20.6	+3.9	0.036	79/64
rrf-3 (pk1426)	*sir-2.1 1/2*	1	17.4/18.1 (±0.51/0.62)	-3.9	0.32	61/61	17.4/18.1	-3.9	0.32	61/61
rrf-3 (pk1426)	*sir-2.1/ acsd-1*	1	17.6/18.1 (±0.56/0.62)	-2.8	0.67	66/61	17.6/18.1	-2.8	0.67	66/61
			17.6/17.4[a] (±0.56/0.51)[a]	+1.1[a]	0.57[a]	66/61[a]				
rrf-3 (pk1426)	*atfs-1 1/2*	2	17.1/17.9 (±0.45/0.46)	-4.5	0.42	135/125	16.8/17.6	-4.5	0.42	69/64
							17.4/18.2	-4.4	0.67	66/61
rrf-3 (pk1426)	*atfs-1/ acsd-1*	2	18.0/17.9 (±0.48/0.46)	+0.6	0.72	117/125	18.2/17.6	+3.4	0.58	55/64
			18.0/17.1[b] (±0.48/0.45)[b]	+5.2[b]	0.25[b]	117/135[b]	17.9/18.2	-1.6	0.94	62/61
rrf-3 (pk1426)	*ubl-5 1/2*	1	17.0/20.6 (±0.3/0.45)	-17.5	<0.0001	68/64	17.0/20.6	-17.5	<0.0001	68/64
rrf-3 (pk1426)	*ubl-5/ acsd-1*	1	17.2/20.6 (±0.34/045)	-16.5	<0.0001	74/64	17.2/20.6	-16.5	<0.0001	74/64
			17.2/17.0[c] (±0.34/0.3)[c]	+1.2[c]	0.36[c]	74/68[c]				
rrf-3 (pk1426)	*daf-16 1/2*	2	15.0/17.8 (±0.41/0.52)	-15.7	<0.0001	80/126	13.4/17.0	-21.2	<0.0001	39/60
							16.4/18.6	-11.8	0.01	41/66
rrf-3 (pk1426)	*daf-16/ acsd-1*	2	14.1/17.8 (±0.34/0.52)	-20.8	<0.0001	99/126	13.0/17.0	-23.5	<0.0001	49/60
			14.1/15.0[d] (±0.34/0.4)[d]	-6.0[d]	0.06[d]	99/80[d]	15.1/18.6	-18.8	<0.0001	50/66
Paraquat experiments										
rrf-3 (pk1426)	*acsd-1* (whole life)	3	7.45/6.85 (±0.14/0.17)	+8.0	0.0034	110/137	8.97/8.57	+4.7	0.014	42/64
							6.42/5.71	+12.4	0.028	47/48
							6.11/5.33	+14.7	0.025	24/35
rrf-3 (pk1426)	*acsd-1 1/2*	2	6.19/5.84 (±0.13/0.15)	+6.48	0.0142	38/44	3.9/3.73	+4.56	0.334	30/32
							6.97/6.68	+4.34	0.043	8/12
rrf-3 (pk1426)	*daf-16/ acsd-1*	1	3.07/3.73 (±0.14/0.15)	-21.49	0.006	47/32	3.07/3.73	-21.49	0.006	47/32
rrf-3 (pk1426)	*acsd-1* (develop)	2	3.55/3.28 (±0.13/0.15)	+8.2	0.0149	73/83	3.43/3.08	+11.4	0.0175	53/52
							3.68/3.48	+5.74	0.0279	20/31
rrf-3 (pk1426)	*acsd-1* (adult)	2	3.68/3.28 (±0.13/0.15)	+12.2	0.0013	69/83	3.7/3.1	+21.4	0.00082	51/52
							3.66/3.48	+5.17	0.005	18/31
Tryptophan supplementation experiments										
rrf-3 (pk1426)	*ev/* Trp 50μM	2	22.3/20.1 (±0.51/0.40)	+10.9	<0.0001	129/173	22.4/20.6	+8.73	0.025	71/91
							22.2/20.4	+8.82	0.001	58/78
rrf-3 (pk1426)	*acsd-1/* Trp 50μM	2	22.7/20.1 (±0.50/0.40)	+12.9	<0.0001	143/173	23.2/20.6	+12.6	0.001	62/91
			22.7/22.3[e] (±0.50/0.51)[e]	+1.79[e]	0.81[e]	129/173[e]	22.2/20.4	+8.82	0.06	81/78

[a]Versus *rrf-3 (pk1426) sir-2.1* ½ (½ denotes condition in which RNAi was diluted by one half with empty vector).
[b]Versus *rrf-3 (pk1426) atfs-1* ½.
[c]Versus *rrf-3 (pk1426) ubl-5* ½.
[d]Versus *rrf-3 (pk1426) daf-16* ½.
[e]Versus *rrf-3 (pk1426) ev/*Trp 50 μM.
Errors are represented as s.e.m. Survival analyses were performed using the Kaplan–Meier method and the significance of differences between survival curves was calculated using the log-rank test (two-sided).

nature research

Corresponding author(s): Johan Auwerx

Reporting Summary

Nature Research wishes to improve the reproducibility of the work that we publish. This form provides structure for consistency and transparency in reporting. For further information on Nature Research policies, see Authors & Referees and the Editorial Policy Checklist.

Statistical parameters

When statistical analyses are reported, confirm that the following items are present in the relevant location (e.g. figure legend, table legend, main text, or Methods section).

n/a	Confirmed	
☐	☒	The exact sample size (*n*) for each experimental group/condition, given as a discrete number and unit of measurement
☐	☒	An indication of whether measurements were taken from distinct samples or whether the same sample was measured repeatedly
☐	☒	The statistical test(s) used AND whether they are one- or two-sided *Only common tests should be described solely by name; describe more complex techniques in the Methods section.*
☒	☐	A description of all covariates tested
☒	☐	A description of any assumptions or corrections, such as tests of normality and adjustment for multiple comparisons
☐	☒	A full description of the statistics including central tendency (e.g. means) or other basic estimates (e.g. regression coefficient) AND variation (e.g. standard deviation) or associated estimates of uncertainty (e.g. confidence intervals)
☐	☒	For null hypothesis testing, the test statistic (e.g. *F*, *t*, *r*) with confidence intervals, effect sizes, degrees of freedom and *P* value noted *Give P values as exact values whenever suitable.*
☒	☐	For Bayesian analysis, information on the choice of priors and Markov chain Monte Carlo settings
☒	☐	For hierarchical and complex designs, identification of the appropriate level for tests and full reporting of outcomes
☒	☐	Estimates of effect sizes (e.g. Cohen's *d*, Pearson's *r*), indicating how they were calculated
☐	☒	Clearly defined error bars *State explicitly what error bars represent (e.g. SD, SE, CI)*

Our web collection on statistics for biologists may be useful.

Software and code

Policy information about availability of computer code

Data collection	Microscopy pictures were acquired with Zeiss LSM 700 Upright confocal microscope (Carl Zeiss AG); Victor X4 plate reader (Perkin Elmer) was used for all the assays requiring absorbance, luminescence or fluorescence quantifications; Parallel Worm Tracker for MATLAB was used for worm tracking; oxygen consumption was measured with Oxygen consumption was measured with the Seahorse XF96 instrument (Seahorse Bioscience); the qPCR reactions were performed using the Light-Cycler system (Roche Applied Science)
Data analysis	GraphPad Prism 6 for Mac OS X (GraphPad Software, Inc.), Fiji (http://imagej.nih.gov/ij; version 1.47b)

For manuscripts utilizing custom algorithms or software that are central to the research but not yet described in published literature, software must be made available to editors/reviewers upon request. We strongly encourage code deposition in a community repository (e.g. GitHub). See the Nature Research guidelines for submitting code & software for further information.

Data

Policy information about availability of data

All manuscripts must include a data availability statement. This statement should provide the following information, where applicable:

- Accession codes, unique identifiers, or web links for publicly available datasets
- A list of figures that have associated raw data
- A description of any restrictions on data availability

The authors declare that all the data supporting the findings of this study are available from the corresponding author upon request. The source data are provided for all the experiments presented in the manuscript; for animal experiments each animal has an attributed identifier

Field-specific reporting

Please select the best fit for your research. If you are not sure, read the appropriate sections before making your selection.

☒ Life sciences ☐ Behavioural & social sciences ☐ Ecological, evolutionary & environmental sciences

For a reference copy of the document with all sections, see nature.com/authors/policies/ReportingSummary-flat.pdf

Life sciences study design

All studies must disclose on these points even when the disclosure is negative.

Sample size	Sample sizes were chosen based on studies with similar experimental design and on the known variability of the assay
Data exclusions	Mice that showed signs of severity, predefined by the animal authorizations, were euthanized and removed from the calculations. For the C. elegans lifespan assays the reasons for censoring were the «exploded vulva» phenotype or worms that crawled off the plate. These reasons were pre-established before the beginning of the experiment.
Replication	All the experiments were repeated at least twice (except for the mouse experiments) and the findings were reliably reproduced.
Randomization	For all the animal experiments mice were randomly allocated to distinct groups
Blinding	Histopathological scoring was performed in a blinded way

Reporting for specific materials, systems and methods

Materials & experimental systems

n/a	Involved in the study
☐	☒ Unique biological materials
☐	☒ Antibodies
☐	☒ Eukaryotic cell lines
☒	☐ Palaeontology
☐	☒ Animals and other organisms
☒	☐ Human research participants

Methods

n/a	Involved in the study
☒	☐ ChIP-seq
☒	☐ Flow cytometry
☒	☐ MRI-based neuroimaging

Unique biological materials

Policy information about availability of materials

Obtaining unique materials	Materials can be requested from JA (admin.auwerx@epfl.ch)

Antibodies

Antibodies used	Proteins were detected using the following specific antibodies: ACMSD (Abcam, ab96081, dilution 1:1000), Actin (Sigma, A5441, dilution 1:2000), acetyl-FKHR (Santa Cruz, sc-49437, dilution 1:1000), FOXO1 (Cell Signaling, 2880, dilution 1:1000), HSP90 (BD transduction laboratories, 610418, dilution 1:2000), Total OXPHOS Rodent Antibody Cocktail (Abcam, ab110413, dilution 1:1000), Tubulin (Santa Cruz, sc-5286, dilution 1:2000), Vinculin (Abcam, ab129002, dilution 1:1000).

Validation	All the antibodies were validated by the manufacturer

Eukaryotic cell lines

Policy information about cell lines

Cell line source(s)	The mouse hepatocytes cell line AML-12 (alpha mouse liver 12) and proximal tubular cell line HK-2 (human kidney 2) were obtained from ATCC
Authentication	All the cell lines purchased from ATCC have been authenticated by morphology, karyotyping and PCR-based approaches
Mycoplasma contamination	All cell lines tested negative for mycoplasma contamination
Commonly misidentified lines (See ICLAC register)	No commonly misidentified cell lines were used

Animals and other organisms

Policy information about studies involving animals; ARRIVE guidelines recommended for reporting animal research

Laboratory animals	For the MCD diet-induced NAFLD model 12 weeks-old C57BL/6J male mice were used, for the Ischemia/reperfusion-induced AKI 9 weeks-old C57BL/6J male mice were used; for the Cisplatin-induced AKI 8-9 weeks-old C57BL/6J male mice were used and for the primary hepatocytes were isolated from 8–12-week-old C57BL/6 mice (both males and females)
Wild animals	The study did not involve wild animals
Field-collected samples	The study did not involve samples collected from the field